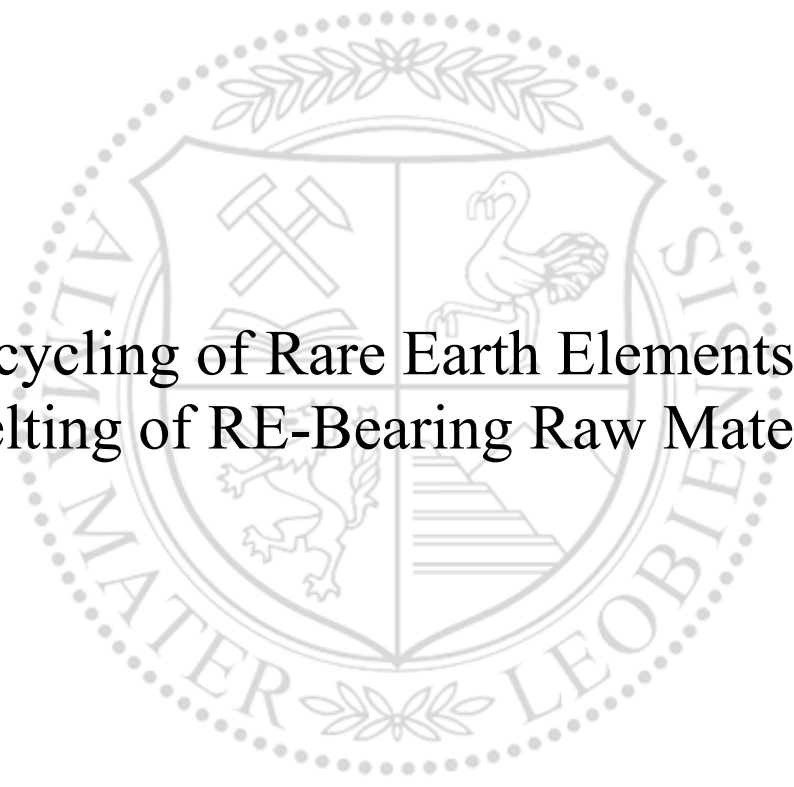




Chair of Nonferrous Metallurgy

Doctoral Thesis



Recycling of Rare Earth Elements by
Smelting of RE-Bearing Raw Materials

Wahyudin Prawira Minwal

July 2023



AFFIDAVIT

I declare on oath that I wrote this thesis independently, did not use other than the specified sources and aids, and did not otherwise use any unauthorized aids.

I declare that I have read, understood, and complied with the guidelines of the senate of the Montanuniversität Leoben for "Good Scientific Practice".

Furthermore, I declare that the electronic and printed version of the submitted thesis are identical, both, formally and with regard to content.

Date 20.07.2023

A handwritten signature in blue ink, appearing to read 'Wahyudin'.

Signature Author
Wahyudin Prawira Minwal

Acknowledgement

Rare earth processing is an important topic for my country, Indonesia, in the last few years. It is an honour opportunity to work and carry out the research in this special university.

Sincere thanks are due to Prof. Stefan Luidold and Prof. Helmut Antrekowitsch, my supervisors, for giving me the topic, his guidance, encouragement and constant support. I am eternally grateful for all valuable discussion and your wisdom. Thanks are also due to Prof. Johannes Schenk, my mentor, and all of professors in Nichteisenmetallurgie for their support and sharing knowledge.

I would like to thank the staff who are always available. In particular, thanks go to Dr. Christoph Sagadin, Dr. Eva Gerold, Mr. Christian Bartelme, Ms. Carmen Schlager, and Ms. Nadine Tatzreiter.

For me, my family is always a source of strength and enjoyment. Words cannot express my thanks to my dear wife, Syari, and my daughter, Safiya, and also Mama(s), Papa(s), my sisters and brothers. For all of them I am always indebted.

I also would like to thank Mas Hafidz (and family), Mas Fahim (and family), Bang Andi, and Keluarga Pengajian Graz for the support and the recipes during my study.

Finally, the financial support of *Österreichs Agentur für Bildung und Internationalisierung* (OeAD) is most gratefully acknowledged. Thank you for giving me the opportunity to study abroad in Leoben, the peaceful city.

Danke schön!

Abstract

Rare-earth elements (REEs) are a group of 17 chemically similar metallic elements (i.e. 15 lanthanides, plus scandium and yttrium), which are strategic for application in modern life. Both the United Nations and the European Union classified REEs as critical and strategic metals due to their properties and their increasing use in critical applications such as wind power plants. Due to large and increasing domestic demand, China, the largest producer of rare earths, has tightened export quotas for rare earth concentrates since 2012. Recycling rare earths from secondary resources such as slag is particularly important to increase resource efficiency, escape scarcity and minimize environmental impacts. The common method for processing REEs is hydrometallurgy. However, the disadvantages of this method are the need for finely ground concentrate and high wastewater generation, which causes significant environmental pollution. Therefore, this method is not recommended for direct recovery of REEs from slags with low REE content. The formation of RE-rich phases by pyrometallurgical processes, such as heat treatment, which are separable from REE-free phases and leachable can be used to enrich RE in the concentrate. The objective of this research is to provide the understanding of the rare earth elements (REEs) extraction process from slag, including the ability of various solid phases to incorporate REEs.

This study applied cerium oxide, CeO_2 , with a purity of 99.9 % as a representative of rare earth oxides (REOs) as they have similar properties both physical and chemical. In addition, several other substances, namely CaO , MgO , SiO_2 , and Al_2O_3 , were also used in some experiments as constituent components of artificial slag. The experiment focused on the dissolution of cerium oxide in the phases of the system $\text{CaO-MgO-SiO}_2(-\text{Al}_2\text{O}_3)$. In this investigation, used contents of CeO_2 were 1 wt.-%, 2 wt.-%, and 5 wt.-%. After determining the initial compositions, the slag sample were prepared and then melted at elevated temperature until the transformation from solid phase to the liquid phase was reached and observed using the hot stage microscope (HSM) with various parameters. Temperature used to melt the slag samples were 1400 °C, 1550 °C, and 1600 °C whereas the holding time of the temperature was varied between 15 minutes and 1 hour. Afterwards, an analysis by a SEM instrument of JEOL JSM IT-300 LV, equipped with energy dispersive X-ray (EDS) served for the determination of type and compositions of the generated phases.

The result shows cerium can be enhanced by forming a Ce-incorporating phase, for instance $\text{Ce}_{9.33-x}\text{Ca}_x(\text{SiO}_4)_6\text{O}_{2-x}$ containing about 58.82–62.85 wt.-% cerium oxide. Lower cerium oxide contents can also be found in some phases such as $\text{Ca}_{2-x}\text{Ce}_x\text{SiO}_{4+\delta}$, CaSiO_3 , $\text{CeCa}_3\text{Si}_6\text{O}_{17}$, $(\text{Ca,Mg})\text{SiO}_3$, $(\text{Ca,Mg,Ce})(\text{Al,Mg})(\text{Al,Si})_2\text{O}_6$. In the tests for the system CaO-MgO-SiO_2 with an initial cerium oxide content of 5 wt.-%, the highest cerium oxide content was reached with 62.85 wt.-% in the phase $\text{Ce}_{9.33-x}\text{Ca}_x(\text{SiO}_4)_6\text{O}_{2-x}$ at 1600 °C for 15 min with a basicity of 1.38. When the basicity is reduced to 0.52, the generated phases are dominated by SiO_2 due to its high content in the initial composition while cerium oxide remains in the matrix. No separation into several phases can be observed from the experiment carried out at basicity of 0.67 as a single homogenous phase resulted. At lower initial CeO_2 contents of 2 wt.-% and 1 wt.-%, no Ce-incorporating phase forms for an increased melting time of 1 hour. When Al_2O_3 is added with a fixed content, cerium oxide can be either incorporated in a certain phase such as $(\text{Ca,Mg,Ce})(\text{Al,Mg})(\text{Al,Si})_2\text{O}_6$ (20.86 wt.-% Ce_2O_3) or remained in the matrix (1.72-5.79 wt.-% Ce_2O_3).

Table of Content

Affidavit	i
Acknowledgement	ii
Abstract	iii
Table of Content	iv
1 Introduction	1
1.1 Aims of Research.....	6
1.2 Research Methodology	6
2 Technical Fundamentals	8
2.1 Processing and Recovery of Rare Earth Elements from Secondary Resources.....	8
2.2 Extraction process of REEs from Metallurgical Slag.....	9
2.3 Processing of REEs from Low REE-Bearing Slag	10
2.4 Enrichment of REEs in Metallurgical Slag	11
3 Experimental Investigations	13
3.1 Sample Preparation	15
3.2 Heat Treatment Process	17
3.3 Phases Characterization	18
3.4 Phases Identification Method	19
4 Results	21
5 Discussion	28
5.1 Experiment Result of Slag Sample 1 after Non-isothermal Treatment at 1550 °C for Melting Time of 1 Hour.....	28
5.2 Experiment Results of Slag Samples with Fixed Composition of CeO ₂ and Varied Composition of CaO, MgO, and SiO ₂ for Melting Time of 15 minutes	29
5.3 Experiment Results of Slag Samples with the Presence of Al ₂ O ₃	31
5.3.1 Experiment Results of Slag Samples with Additionally Containing Al ₂ O ₃ with Varied Concentrations of CeO ₂ at 1600 °C for a Melting Time of 15 Minutes.....	31

5.3.2	Experiment Results of Slag Samples with Additionally Containing Al_2O_3 with Varied Compositions of CeO_2 at 1600 °C for a Melting Time of 1 Hour	32
5.4	Experiment Results of Slag Samples with Varied Composition of CeO_2 for Melting Time of 1 hour without the Presence of Al_2O_3	33
5.5	Diagram of the System $\text{CaO-MgO-SiO}_2\text{-Ce}_2\text{O}_3$ at Room Temperature	33
6	Conclusion.....	35
7	Bibliography	36
8	List of Figures	42
9	List of Tables	43
10	Appendix.....	44
10.1	Appendix A – Data of Heat Treatment Process of the Slag Samples in Hot Stage Microscope	44
10.2	Appendix B – Measured Data of the Slag Samples	52

1 Introduction

Rare-earth elements (REEs) are a group of 17 chemically similar metallic elements (i.e. 15 lanthanides, plus scandium and yttrium), which are strategic for application in modern life. REEs only have similar electron configurations but exhibit distinctive physical and chemical properties which enable their use in a broad range of technologies [1]. Consequently, REEs can be used in a wide range of applications such as magnets, catalysts, metallurgical additives, batteries, polishing powders, phosphors, glass additives, and ceramics. Distribution of REEs in each application is not the same, depending on manufacturers but the percentages can be estimated as shown in Table 1. The United Nations as well as the European Union listed REEs as critical and strategic metals because of their properties and increasing usages in critical application such as for wind power plants [2]. REEs can be categorized into two groups, namely light REEs (LREE) and heavy REEs (HREE). At present, the LREE market is dominated by the demand for Nd for neodymium-iron-boron magnet (NdFeB) magnets. Whereas HREE market is driven by the demand for Dy for NdFeB magnet due to its capability to increase magnetic coercivity and subsequently, increases high temperature performance and resistance to demagnetization [3].

Table 1. Distribution of REEs in many applications [4]

Application	La (%)	Ce (%)	Pr (%)	Nd (%)	Sm (%)	Eu (%)	Gd (%)	Tb (%)	Dy (%)	Y (%)	Other (%)
Permanent magnets			23	69			2	1	5		
Battery alloys	50	34	3	10	3						
Metallurgy	26	52	5	17							
Auto catalysts	5	90	2	3							
Fluid catalytic cracking	90	10									
Polishing powders	31	65	4								
Glass additives	24	66	1	3						2	4
Phosphors	9	10				5	2	5		69	
Ceramics	17	12	6	12						53	

Rare earth minerals are so many in number but there are six minerals which can be categorized as primary resources of REEs i.e., bastnaesite $[(Ce,La)(CO_3)F]$, monazite $[(Ce,La,Th)PO_4]$, xenotime (YPO_4) , loparite $[(Ce,Na,Ca)(Ti,Nb)O_3]$, apatite $[(Ca,REE,Sr,Na,K)_3Ca_2(PO_4)_3(F,OH)]$, and ion adsorption clays. The first three minerals are known as world rare earth resources and commercial rare earth minerals which have composition of 70-75 % REO, 55-60 % REO, and 55-60 % REO, respectively [5], [6]. Rare earths occur around the world but are mostly mined and extracted in China. They are also mined in other countries such as Australia, India, and United State but only slowly growing. Due to large and increasing domestic demands, China has been tightening export quota of REE concentrate since 2012. This may cause serious problems for REE users outside of China as well as for the development of a more sustainable, low-carbon economy [7]. In 2013, China had about 50 % of the rare earth ore reserves and dominated rare earth mining with around 90 %. Figure 1 shows the world's rare earth producing mines in 2013.



Remarks: 1 = Bayan Obo, China; 2 = Rare earth cation clays, China; 3 = Mount Weld, Western Australia; 4 = Vizag, Andhra Pradesh, India; 5 = Manavalakurichi, Tamil Nadu, India; 6 = Chavara, Kerala, India; 7 = Lovozerskoy, Russia; 8 = Mountain Pass, California; E = Kuantan, Malaysia (Extraction Plant)

Figure 1. The world's rare earth producing mines in 2013 [8]

There are several steps of REEs processing from primary resources which comprise deposit exploration, mining, beneficiation, chemical treatment, separation, refining, and purification [5]. In metallurgical processes, REEs extraction is generally initiated by a beneficiation process to remove undesired impurities and to enhance the concentration of REEs in concentrate. Physical beneficiation techniques which have been proved to enrich REEs from primary resources are gravity concentration, tabling, flotation, magnetic separation, and high tension separation [6], [9], [10]. For instance, magnetic separator is commonly used to separate highly magnetic gangue from non-magnetic minerals such as monazite and xenotime.

In REEs extraction process from primary resources, hydrometallurgical processes are commonly used over pyrometallurgical ones. The rare earth extraction by hydrometallurgical route uses one or more reagents to decompose the minerals and to dissolve the rare earth elements into solution. These reagents are mainly inorganic acids, alkalis, electrolytes, and chlorine gas. The commonly used acids include sulfuric acid (H_2SO_4), hydrochloric acid (HCl), and nitric acid (HNO_3). Whereas sodium hydroxide (NaOH) and sodium carbonate (Na_2CO_3) are the most common alkalis. Electrolytes include ammonium sulfate ($(\text{NH}_4)_2\text{SO}_4$), ammonium chloride (NH_4Cl), and sodium chloride (NaCl). Several factors affecting the extraction process are type of minerals in concentrate, grade of concentrate and characteristics of targeted products.

Separation of REE is a complex process because it relies on small differences in chemical properties, such as the solubility and chemical stability [11]. Many researchers studied several methods to separate them into individual elements such as fractional precipitation and crystallization, ion-exchange, and solvent extraction also called liquid–liquid extraction. Solvent extraction is currently the dominant technology of separating and purifying the individual rare earth elements [10].

The main issue of producing REEs from primary production is the so-called balance problem. Some REEs will be produced in larger quantities than required by the REE market. Then, these elements need to be stockpiled which comes at a cost. In this condition, for instance, REEs production is dominated by Lanthanum (La) and Cerium (Ce) while the demand of REE is for Neodymium (Nd) and Dysprosium (Dy). Therefore, the demand for Nd and Dy might not be met by primary production alone. The balance problem implies that the rare earths industry will either have to find new applications for REEs that are excessively available or need to find substitutes for REEs that have both limited availability and high demand. This issue can be partly overcome by recycling. Potential secondary resources include residues from both primary and secondary metal production of which the volumes are enormous so the content of REEs is also very large and may secure an independent source as well as shield REEs resource-poor countries from export quotas and price fluctuations as illustrated in Figure 2.

Table 2. Potential sources of REEs recycling [1]

Source for recycling	Targeted REEs
Catalyst in chemical and petroleum industry	LREE (La, Ce)
End of Life products	La, Ce, Tb, Y
Magnets	Nd, Dy, Pr, and Tb
Batteries	La, Ce, Pr, and Nd
Other industrial processes and residues	Depending on the source material, the recycling process can target different REE

Compared to primary processing, recycling of rare earth from secondary resources will provide more benefits with respect to air emissions, groundwater protection, the risks of acidification, eutrophication, and climate protection. The basic processes used for recycling of rare earth from secondary resources are similar to those utilized for extraction of rare earth from ores [14]. In REEs extraction processes from primary resources, hydrometallurgical methods are commonly used over pyrometallurgical techniques. Hydrometallurgy processes are more reliable due to a possibility of selective leaching of rare earth from low-grade metal resources with lower processing cost and relatively low pollutant generation [15]–[21]. However, the disadvantages of this process are the demand of finely ground concentrate and the large scale of wastewater generated that cause a serious environmental pollution. Therefore, it is very important to enhance rare earth elements concentration in slag prior to hydrometallurgical processes.

In comparison to natural ores, slags have the advantage that the formation of mineral phases during cooling can be influenced by use of different slag formers, cooling rates and furnace conditions. This processing of slags is defined as hot stage slag engineering [22]. The slag composition and microstructure can be changed by adjusting the primary pyrometallurgical process directly or immediately after separation of the slag from the molten metal, while the slag is still at high temperature. If a metal can be enriched in a certain mineralogical slag phase embedded in a matrix of other minerals by choosing a suitable slag composition and cooling trajectory, then a separation of this mineral phase might be possible by conventional ore processing methods. Furthermore, rare earth oxides can be selectively separated from the slag by hydrometallurgical processes.

1.1 Aims of Research

This research project is aimed to consolidate the understanding of extraction process of rare earth elements (REEs) from slag. Specifically, a series of experiment was carried out in variations of initial composition of substances to produce an artificial slag. Melting time and Al_2O_3 as flux are used as parameters of experiment, which aimed at:

- Ability of various solid phases to incorporate REEs.
- Reviewing best conditions of heat treatment and additives to obtain a REE-rich phase which is easily separable and leachable as well as contain sufficient high content of REEs.

1.2 Research Methodology

This research is based on the fact that hydrometallurgy is the most commonly used process to extract rare earth elements (REEs) from secondary resources such as metallurgical slags. However, processing materials with low REEs contents requires a large amount of chemicals and water as well as poses a massive problem, especially in terms of the environment [23] [24]. This process can generate large amounts of residues and wastewater. Therefore, this method is not recommended for recovering REEs directly from slag. Pyrometallurgical technology has been reviewed as an alternative to process REEs from slag which offers following advantages such as high processing capacity, simple process, high efficiency, less production of pollution and hazardous wastes [25].

The first stage of the research comprises a literature review which is focused to understand and strengthen fundamental aspects of theory related to experiment through a comprehensive literature survey. Operational mechanism of instruments in order to characterize REEs are also studied such as hot stage microscope (HSM) and scanning electron microscope (SEM).

The next stage deals with several experiments regarding phase formation using HSM and SEM. In the experiments, cerium was used as a representative of REEs due to their similar properties. These investigations are carried out at different initial compositions, temperatures, and fluxes as parameters of the process. By the experiments, solid phases are identified that easily incorporate REEs in significant concentrations as well as others which do not or only to a minor content dissolve them. The expected results form the knowledge base for a partitioning of the slag into a REE concentrate and a gangue without relevant amounts of REEs. Research methodology conducted in the investigation is shown in Figure 3.

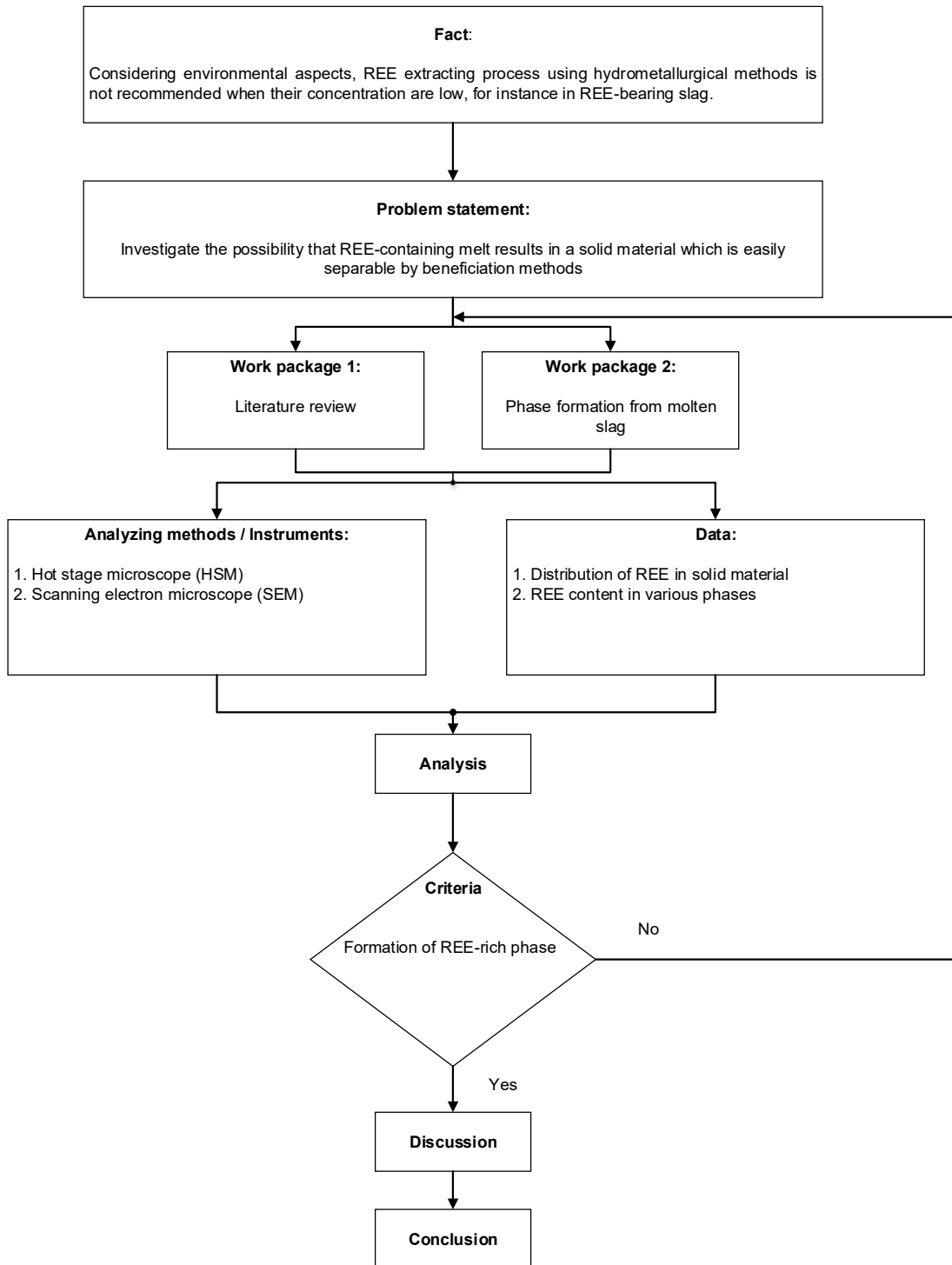


Figure 3. Research methodology

2 Technical Fundamentals

This chapter deals with the fundamental aspects used to build the research. The discussion starts with the processing and extraction of rare earth elements (REEs) from secondary sources, and is complemented by the extraction process of rare earth elements from metallurgical slags. The REEs in metallurgical slags from recycling pose a problem of low concentration. Consequently, the method to enhance the REEs content as an alternative prior to recovery with hydrometallurgical processes has to be discussed.

2.1 Processing and Recovery of Rare Earth Elements from Secondary Resources

The recycling that takes place can be divided into three groups, namely direct recycling of production scrap or residues, urban mining of end-of-life (EOL) products, and recycling or landfill mining of industrial solid and liquid wastes containing REEs. This concept is referred to as "technospheric mining," as shown in Figure 2. The recovery of rare earths by technospheric mining has the advantage that there are no thorium problems, and the composition of the recovered rare earth concentrate is less complex [26], [27]. The lack of cost-efficient processing of primary deposits forces many countries to rely on recycling of rare earth elements. The recycling must meet various aspects, such as an economic perspective, meeting the collection, transportation, and processing cost requirements for electronic recycling [27]. Rare earths recycling from secondary resources is very important to increase resource efficiency, escape scarcity, consume less energy than primary rare earths production, minimize the expansion of land filling, and reduce environmental impact [8], [13]. In 2014, the recycling rate of rare earths amounted to only 1-2 % of their end-use objects. This is a big difference from the recycling rates of other metals such as 90 % for iron and steel, 80 % for platinum group metals, 70 % for aluminum, and 60 % for copper.

Several authors classify scrap used as a source for rare earths recycling into two categories, namely scrap generated from mechanical processing in the manufacturing process and scrap generated from physical disassembly of EOL products [28]–[30]. The recycling process for rare earths from end-of-life products includes four main steps, namely collection, disassembly, separation, and processing [14], [31]. Collection can be done by various means. Collection methods include direct shipment of products to sites set up by equipment manufacturers and drop-off of used products at designated sites, such as retail stores or sites specifically set up as part of collection campaigns. Disassembly/preprocessing steps are critical to separate the high-value components from the lower-value materials. Often, high-value materials such as

rare earths and other metals like gold make up only a small percentage of the item being recycled, and separation steps allow them to be recovered more efficiently. However, even when metals are separated from other non-metallic components, mixed metal scrap is more difficult to recycle than separated metals. Typical disassembly and processing steps include manual or mechanical disassembly, manual or mechanical separation, mechanical crushing, and screening. The goal of this step is to remove hazardous and unwanted materials while retain the valuable materials for reuse and recycling processes. After the pre-processing steps are completed, the components of interest are ready for the processing step.

2.2 Extraction process of REEs from Metallurgical Slag

Metallurgical processes produce various slags as a by-product. Depending on their origin and properties, slags can be divided into three groups namely ferrous slags, nonferrous slags, and combustion slags [32]. There are different types of nonferrous slags produced by nonferrous metal smelters, such as tin, copper, zinc, and nickel. Extensive studies on metal recovery from nonferrous slags have been conducted in the past decades. However, reports on the recovery of rare metals and rare earths from nonferrous slags are relatively sparse. The recovery of niobium (Nb) and tantalum (Ta) from tin slag was reported by [33]. Recently the investigation results on the recycling of rare earth metals from phosphorus slag were reported by [34].

Pyrometallurgical flowsheets for recycling valuable metals from batteries can produce a slag that is relatively rich in rare earths. The batteries are placed in a vertical shaft furnace along with a small amount of coke and a slag former [35]. Oxygen-enriched air is injected into the bottom of the shaft furnace. The metals are converted into a Ni-Co-Cu-Fe alloy and a slag. The slag consists mainly of oxides of calcium, aluminum, silicon, and iron, and also contains lithium and rare earths [36]. Compared to natural ores, slags have the advantage that the formation of mineral phases during cooling can be influenced by using different slag formers, cooling rates, and furnace conditions. This processing of slags is referred to as hot stage slag engineering [22].

The effects of slag composition, slag to metal (S/M) ratio, and scrap type on rare earth slag extraction were studied [30]. In general, a lower amount of slag used results in a higher REE concentration in the slag. Slag composition and microstructure can be altered by adjusting the primary pyrometallurgical process immediately or after the slag is separated from the molten metal while the slag is still at high temperature. If a metal can be enriched in a particular mineralogical slag phase embedded in a matrix of other minerals by choosing an appropriate slag composition and cooling course, then separation of this mineral phase by conventional ore processing techniques might be possible. In addition, rare earth oxides can be selectively separated from the slag by hydrometallurgical processes.

In hydrometallurgical processes for the recovery of rare earths from slag, there are two main steps, namely dissolution of the rare earths and separation. The extraction and separation of rare earths and Al from FCC waste slag achieved by acid leaching and selective precipitation were studied by [37]. Under the optimum leaching conditions, nearly 91.01 % La, 92.24 % Ce and 94.77 % Al were extracted from FCC waste slag. The separation of rare earths happened by adding Na_2SO_4 to precipitate the rare earths in the form of $\text{NaRE}(\text{SO}_4)_2 \cdot x\text{H}_2\text{O}$, while Al remained in the leachate. The recovery of REEs from molten NiMH battery slag was investigated [8]. This method consists of several steps, i.e., (i) the slag is granulated with water to form particles with a diameter of about 100 μm , (ii) very finely ground, (iii) leached with nitric or hydrochloric acid, and (iv) purified and separated into individual rare earth solutions by solvent extraction. Leaching and recovery of the pure rare earths takes place at Solvay's rare earths plant in La Rochelle, France.

2.3 Processing of REEs from Low REE-Bearing Slag

REEs can be found not only as main elements in primary ore, but also as by-products of metal processing. The Bayan Obo Mine is known to be the world's largest REE deposit in which low concentration of REEs coexist with iron, niobium, and other metals, with only a few hundred parts per million by weight. Therefore, an economic and efficient extraction of REEs from the ore is difficult. The Bayan Obo facility primarily produces iron with large amounts of slag containing REEs at high concentrations [38], [39]. Unlike Bayan Obo, in Indonesia, REEs are found in monazite and xenotime minerals and end up in the final slag of tin metal processing. Typically, the slag contains 5-6 % of REEs which comprises 3 % LREE and 2.5 % HREE. This slag is processed to produce RE concentrates containing REO up to 97 %. However, the concentration process consists of complex processes and requires longer time and much energy [40]. Therefore, treatment of REE-bearing slags by a pyrometallurgical route is a potential alternative to separate REEs from other elements prior to any extraction process using chemicals.

Due to low concentration of REEs in the slag, a pretreatment process for slag, followed by magnetic separation, flotation or supergravity separation, namely, selective crystallization and phase separation, have been more effective in increasing rare earth grades [41]. Furthermore, rare earth phase crystallization is crucial to study in order to enrich RE-elements and generate RE-phase growth well. Crystallization behavior of $\text{CaO-SiO}_2\text{-CaF}_2\text{-La}_2\text{O}_3$ rare earth-containing slag using selective crystallization and phase separation (SCPS) was studied by [39].[42] Influence of P_2O_5 and CaF_2 on crystallization phase in $\text{CaO-SiO}_2\text{-Al}_2\text{O}_3\text{-La}_2\text{O}_3$ slag system was investigated by [41]. Precipitation of RE-slag by isothermal reduction and melting separation

was studied by [43]. However, effect of composition of the slag on crystallization behavior has not been investigated.

2.4 Enrichment of REEs in Metallurgical Slag

Extraction of REEs from RE-bearing secondary resources such as metallurgical slags is dominated by hydrometallurgical methods exemplarily described in [23], [44], [45]. However, it requires large amounts of chemicals and water resulting in large amounts of waste sludges and wastewater [12]. Thus, it seems not effective to extract REEs from sources with low concentration. Forming of RE-rich phases by pyrometallurgical method can be used to enrich RE in concentrate as can be seen in Figure 4, in which fundamental understanding of RE distribution in slag, appropriate cooling path as well as the influence of process parameters such as temperature and atmosphere exhibit important roles [46], [47]. In addition, the structures, compositions and transformation of REEs phases are also relevant [38]. In NiMH batteries recycling, FeO-B₂O₃ fluxes were used as REEs oxidant at high temperature so that 99 wt.-% REEs were separated and collected in an oxide phase [48]. Selection of a suitable slag system is a crucial point which has to fulfill demands such as high-density difference to the liquid metal, low viscosity and pour capacity [49]. Calcium oxide and silica are commonly used as fluxes in metallurgical industries and in general have very high content in slags affecting the properties of slag systems [25]. Chemical compositions and mineralogy of RE-phases in RE-bearing slags can be found different from each other. Various research has investigated the formation of RE-phases in Bayan Obo RE-bearing slag. RE-phases can be formed during the cooling process such as calcium cerite (RE₂O₃-CaO-SiO₂), britholite (Ca₃Ce₂[(Si,P)O₄]₃F), or cerium fluorosilicate (7[(Ca,Ce)₂SiO₄](F,O)₁₀) [50]–[52]. Crystallization behavior of RE-phases affected by temperature and cooling mechanism represents a critical factor for the recovery of REE from slag [24]. During isothermal process, the volume fraction of RE-phase increased significantly with the elongation of the holding time [53]. Therefore, it is essential to study the isothermal phase equilibria of RE-bearing systems such as Ce₂O₃-CaO-SiO₂ system at 1300 °C, 1500 °C, and 1600 °C [24], [54]. Ce₂O₃ performs as a basic component in the Ce₂O₃-CaO-SiO₂ system [54].

After a RE-rich phase is obtained and separated from others, the next step comprises the recovery of REE using hydrometallurgical methods. There are two main steps namely the dissolution of REEs and the separation by selective processes. There are several important parameters in leaching processes of rare earth from waste slag [55]. Increasing leaching temperature will accelerate the leaching rate and extent of leaching of lanthanum from the slag [15]. An extraction and separation of REEs and Al from fluid catalytic cracking (FCC) waste

slag were achieved by acid leaching and selective precipitation. Under the optimum leaching conditions, almost 91.01 % of La, 92.24 % of Ce, and 94.77 % of Al in the FCC waste slag was extracted [37]. Leaching of REE from phosphorus slag using nitric acid performed good results with recovery efficiencies of 98.3–98.6 % for rare earth metals, 96.5–98.6 % for aluminum, 94.9–96.5 % for iron, and 99.1–99.5 % for calcium [56]. The recovery of REEs from NiMH battery molten slags were studied. This method consists of several steps i.e. (i) the slag is water-granulated to 100 μm diameter particles; (ii) ground very fine; (iii) leached with nitric or hydrochloric acid; and (iv) purified and separated into individual rare earth solutions by solvent extraction [8].

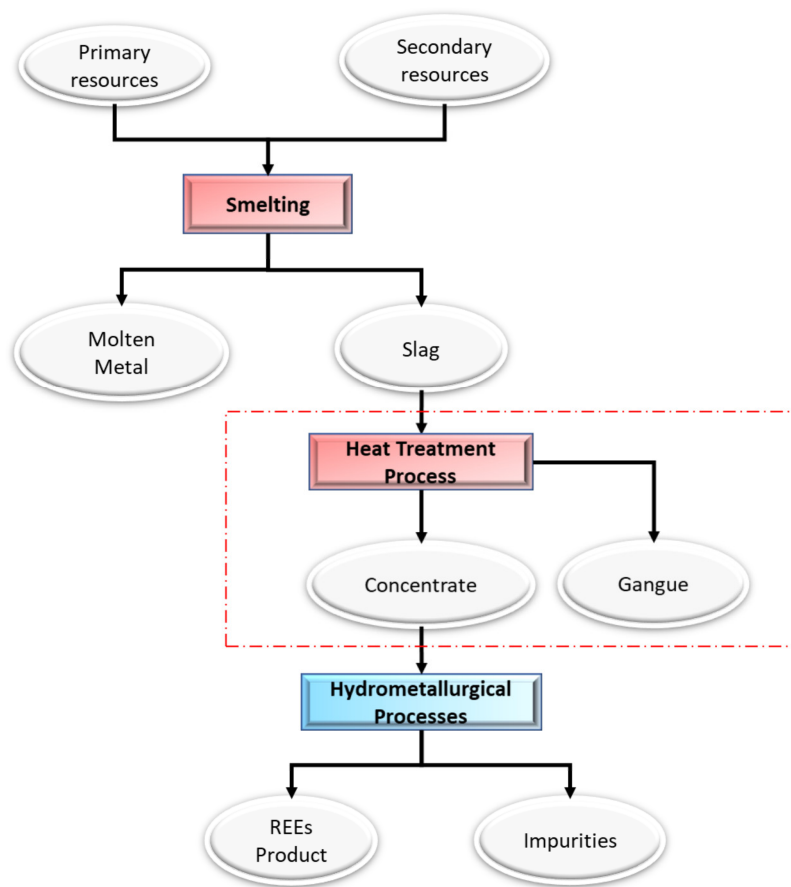


Figure 4. Schematic process of REE enrichment in slag through heat treatment process

3 Experimental Investigations

In this chapter, the steps carried out in the experimental procedure are explained. This study applied a cerium oxide, CeO_2 , with a purity of 99.9 % as representative of rare earth oxides (REOs) as they have similar properties both physical and chemical. In addition, several other substances were used, namely magnesium oxide (MgO), calcium oxide (CaO) and silicon oxide (SiO_2) mixed with CeO_2 to generate synthetical slags. Aluminum oxide (Al_2O_3) was also used in some experiments as component. Furthermore, the experiment focused on the slag phase formed in the ternary system constructed with Factsage8.0. Furthermore, the experiment focused on the dissolution of cerium oxide in the phases of the system $\text{CaO-MgO-SiO}_2(-\text{Al}_2\text{O}_3)$. An isothermal section of this ternary diagram was calculated by Factsage 8.0 at 1500 °C to select compositions of slags, which can be completely melted in the applied hot stage microscope. The selected six test points, used in experiments, are pointed out by green marks in Figure 5. The addition of a certain amount of CeO_2 resulted in the definite composition of the slag samples for the melting experiments, which are summarized in Table 3.

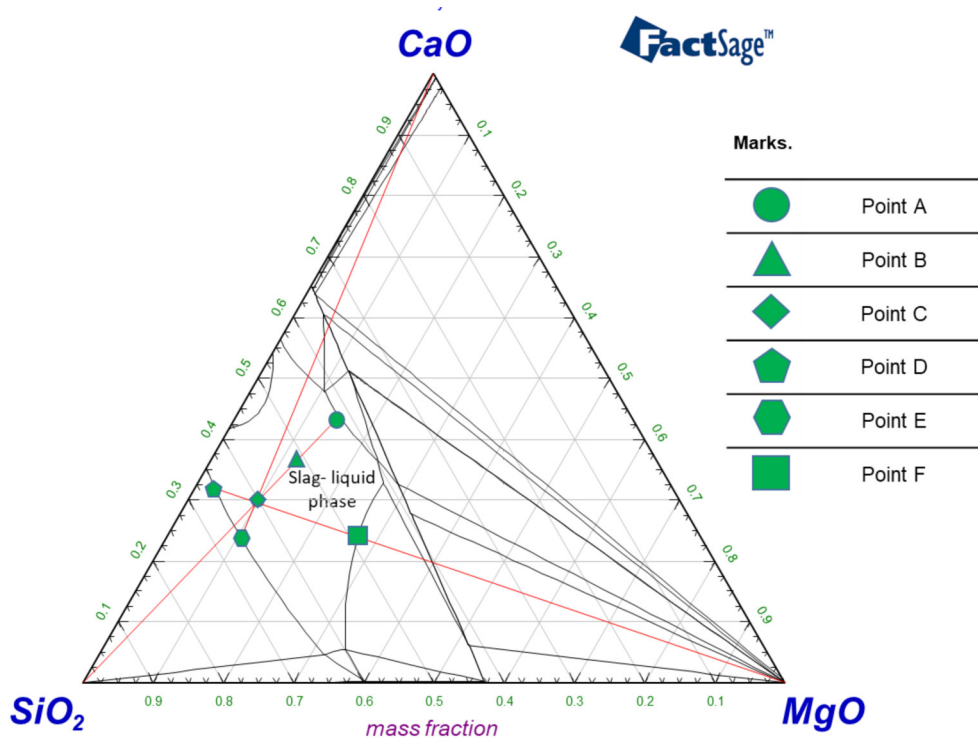


Figure 5. Ternary system of CaO-MgO-SiO_2 at 1500 °C and 1 atm constructed using Factsage 8.0 in which an area with only liquid slag as stable phase was observed from which six test points were selected

The experimental process consisted of four main steps namely calculation of initial compositions, preparation of slag samples, high temperature melting process, and phase characterization. After the determination of initial compositions, the slag sample were prepared and then tested in a series of experiments with various parameters. The melted slag samples obtained from the tests were further prepared in the embedding process in which the melted slag samples were mounted into the resin. An analysis through scanning electron microscopy and energy dispersive X-ray spectroscopy (SEM-EDS) served for the determination of type and compositions of the generated phases. The entire sequence of the test procedures is shown in Figure 6.

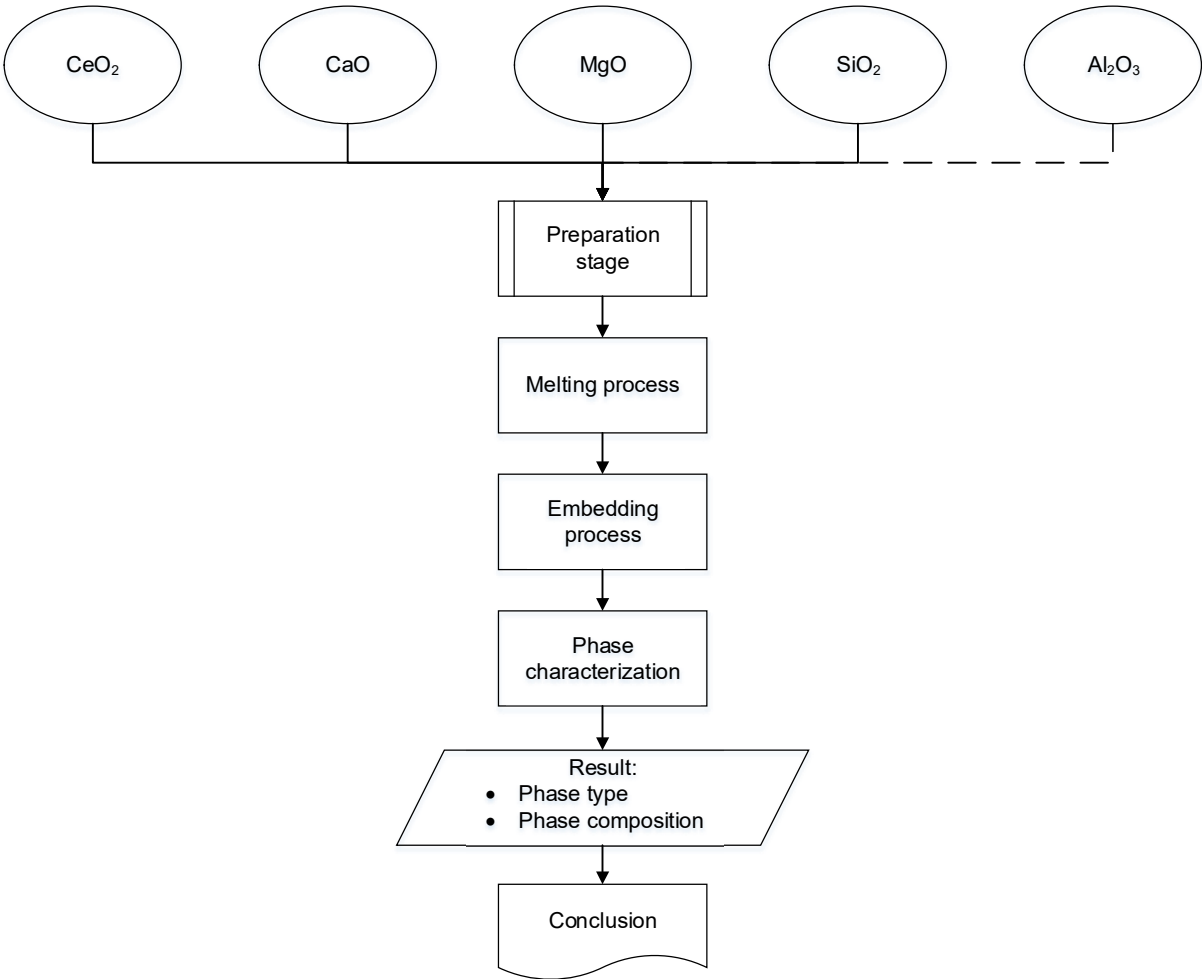


Figure 6. Flowchart of sequence of the test procedures

3.1 Sample Preparation

The aim of the sample preparation was to obtain a homogeneous slag material as a feed of the further test. The preparation started with weighting of each oxide of CeO_2 , CaO , MgO , and SiO_2 as well as Al_2O_3 according to the calculation of the initial compositions required for the melting test. This investigation used the raw materials CeO_2 (CAS Nr. 1345-13-7), CaO (99.9 pct, Sigma-Aldrich, CAS Nr. 1305-78-7), MgO (≥ 98 pct, Roth, CAS Nr. 1309-48-4), SiO_2 (> 99 pct, Roth, CAS Nr. 14808-60-7), and Al_2O_3 (≥ 99 pct, Roth, CAS Nr. 1344-28-1) (see Figure 7). Before weighting of Al_2O_3 , an additional treatment took place by heating the raw material up to $1400\text{ }^\circ\text{C}$ for 24 hours in the furnace to ensure the aluminum oxide used in the experiment exists as Al_2O_3 . The weighting was conducted with the equipment of Denver Instrument SI-603A that has an accuracy of 0.001 gr.



Figure 7. Raw oxide materials used in the investigations, (a) calcium oxide, CaO ; (b) magnesium oxide, MgO ; (c) silicon dioxide, SiO_2 ; (d) aluminum oxide, Al_2O_3 ; and (e) cerium dioxide, CeO_2

Afterward, all substances were grinded and mixed using a swing mill as shown in Figure 8. Moreover, the use of the swing mill aimed to produce a homogeneous slag sample. The weight of each slag feed prepared for melting test amounted to 100 grams. Finally, the slag feed was ready for further test of the melting process.



Figure 8. Swing mill used in the preparation stage in order to obtain a homogenous slag feed

The first melting test applied an initial composition of 15 wt.-% CeO_2 , 45 wt.-% CaO , and 40 wt.-% SiO_2 . Moreover, melting tests were performed at 6 different points on the ternary diagram of system CaO-MgO-SiO_2 referring to Figure 5. The slag samples of each test point composed of different composition of CaO , MgO and SiO_2 . In this investigation, contents of CeO_2 used were varied of 1 wt.-%, 2 wt.-%, and 5 wt.-%. By addition of CeO_2 , the new oxide compositions were obtained and then used as the initial compositions as shown in Table 3.

Table 3. Initial compositions of slag samples and parameters of melting process

Slag sample	Test point	Initial composition (wt.-%)					Temperature (°C)	Time (hour)
		CeO ₂	SiO ₂	CaO	MgO	Al ₂ O ₃		
1		15.00	40.00	45.00			1550	1
2	C	5.00	57.00	28.50	9.50		1400	0.25
3	A	5.00	39.90	40.85	14.25		1600	0.25
4	D	5.00	62.70	22.80	9.50		1600	0.25
5	E	5.00	62.70	30.40	1.90		1600	0.25
6	C	5.00	57.00	28.50	9.50		1600	0.25
7	B	5.00	49.03	34.89	11.09		1600	0.25
8	F	5.00	46.30	22.86	25.83		1600	0.25
9		5.00	37.80	38.70	13.50	5.00	1600	0.25
10		2.00	39.06	39.99	13.95	5.00	1600	0.25
11		1.00	39.48	40.42	14.10	5.00	1600	0.25
12		5.00	37.80	38.70	13.50	5.00	1600	1
13		2.00	39.06	39.99	13.95	5.00	1600	1
14	C	2.00	58.80	29.40	9.80		1600	1
15	C	1.00	59.40	29.70	9.90		1600	1
16	A	1.00	41.58	42.57	14.85		1600	1

3.2 Heat Treatment Process

In the heat treatment process, the homogeneous slag samples obtained from the preparation stage were melted at high temperature for a certain melting time. Temperature used to melt the slag samples were 1400 °C, 1550 °C, and 1600 °C whereas the holding time of the temperature was varied between 15 minutes and 1 hour. The aim was to investigate the best conditions for producing a cerium-incorporating solid phase, so that an enrichment of cerium in one of several stable phases contained in the slag after solidification and cooling was possible through conventional separation process. The slag was melted at high temperature until the transformation from solid phase to the liquid phase was reached and observed using the hot stage microscope (HSM). Figure 9 shows the hot stage microscope applied to observe melting behavior of slag samples. The melting process consisted of several steps. Firstly, the slag sample was pressed into a small cylinder and placed on a platinum plate. Then, the heating of the sample took place in the instrument with a heating rate of 10 °C/min up to the specified temperature of 1400, 1550, or 1600 °C. After maintaining this temperature for a certain time (15 min or 1 hour) a controlled cooling down to 1100 °C took place with a cooling rate of 2 °C/min before switching off the heater for further cooling to room temperature. During this whole cycle, the furnace chamber was purged by air to control its atmosphere. Finally, the

heat treated sample could be removed for subsequent analysis. The detailed data of heat treatment process of each slag sample in hot stage microscope were given in Appendix A.



Figure 9. Hot stage microscope used to observe melting behavior of slag samples

3.3 Phases Characterization

Prior to metallographic analysis, the melted slag obtained from the heat treatment process was initially prepared by an embedding process. The samples were mounted in resin, with the ratio of resin to hardener being 5:1. Each specimen was placed transversely in the resin so that the analysis would observe the cross-section layer. Afterwards, the mounted resin was left for 48 hours to achieve good hardness. In order to obtain a flat surface, grinding with sandpaper starting from size of 320 to 4000 grit took place. Finally, the mounted resin was washed with isopropanol to clean the surface and then dried in the oven.

The next step comprised metallographic analysis using scanning electron microscope (SEM). The mounted-resin sample were coated with a carbon film for a cross-section observation through SEM. This investigation applied a SEM instrument of JEOL JSM IT-300 LV, equipped with energy dispersive X-ray (EDS) as shown in Figure 10. The analysis was conducted to determine the cerium oxide content of all phases formed during the heat treatment. In addition, the contents of the other elements in each phase, in wt.-%, were also quantitatively determined by EDS.



Figure 10. Scanning Electron Microscope (SEM) equipped with an energy dispersive X-ray (EDS) detector used in the investigation

3.4 Phases Identification Method

The identification of the phases was done based on the calculation of the atomic percentage of the phase constituent elements. The composition of each element, in wt.-%, which has been collected from the EDS analysis was converted to moles of element referring to Equation 1. Cerium, silicon, calcium, magnesium, and aluminum were the elements used for the calculation. In addition, the mole numbers was used to calculate the moles of oxide, taking into account the number of ions contained in the oxide as in Equation 2. Finally, the percentage value of each oxide was calculated by dividing moles of oxide to total of moles of oxide according to equation 3.

$$\text{Moles of element (i)} = \frac{\text{mass of element (i) in wt.-%}}{\text{relative atomic mass of element (i)}} \quad (\text{eq. 1})$$

For reaction of element, $I_xO_y = xI + yO$

$$\text{Moles of oxide (i)} = \frac{\text{Moles of element (i)}}{\text{Number of ion (I),x}} \quad (\text{eq. 2})$$

$$\text{Atomic percentage (i)} = \frac{\text{Moles of oxide (i)}}{\sum_i^n \text{Moles of oxides}} \quad (\text{eq. 3})$$

For instance, identification of cerium phase as cerium oxide was calculated as follows.

$$\text{Moles of Ce} = \frac{\text{mass of Ce in wt. } -\%}{140.116 \text{ g/mol}}$$

Relative atomic mass of Si, Ca, Mg, and Al used in calculation were 28.0855, 40.078, 24.305, and 26.981 g/mol, respectively.

For reaction of cerium dioxide, $\text{Ce}_2\text{O}_3 = 2 \text{ Ce} + 3 \text{ O}$

$$\text{Moles of Ce}_2\text{O}_3 = \frac{\text{moles of Ce}}{2}$$

$$\text{Atomic percentage (Ce}_2\text{O}_3) = \frac{\text{moles of Ce}_2\text{O}_3}{\text{moles of Ce}_2\text{O}_3 + \text{moles of SiO}_2 + \text{moles of CaO} + \text{moles of MgO} + \text{moles of Al}_2\text{O}_3}$$

The same procedure served for the calculation of the atomic percentage of SiO_2 , CaO , MgO , and Al_2O_3 . Finally, identified phases were then validated to appropriate references.

4 Results

The experimental results of the metallographic analysis are presented in this chapter. As mentioned above the experiments were focused on slag liquid area in the ternary system of CaO-MgO-SiO₂ at 1500 °C and 1 atm. Specifically, there were 6 test points at which experiments were carried out as shown in Figure 5. Compositions of phases in the quenched slag samples are given in Table 4.

Table 4. Compositions of phases in the quenched slag samples

Slag sample	Initial composition (wt.-%)					Phase	Final composition (wt.-%)				
	CeO ₂	SiO ₂	CaO	MgO	Al ₂ O ₃		Ce ₂ O ₃	SiO ₂	CaO	MgO	Al ₂ O ₃
1	15.00	40.00	45.00			Ce _{9.33-x} Ca _x (SiO ₄) ₆ O _{2-x} (*)	58.82	23.54	17.64		
						Ca _{2-x} Ce _x SiO ₄₊₅ (*)	11.31	32.81	55.88		
						CaSiO ₃ (**)	6.89	43.73	49.38		
2	5.00	57.00	28.50	9.50		Ce ₂ Ca ₃ Si ₆ O ₁₇ (*)	35.23	42.96	21.81	0.00	
						CaMgSi ₂ O ₆	0.00	55.40	25.88	18.73	
						(Ca,Mg)SiO ₃	0.00	53.01	44.18	2.82	
3	5.00	39.90	40.85	14.25		Ce _{9.33-x} Ca _x (SiO ₄) ₆ O _{2-x} (*)	62.85	22.87	14.28	0.00	
						Ca ₂ MgSi ₂ O ₇	0.00	43.78	41.55	14.68	
						Ca ₃ MgSi ₂ O ₈	0.00	36.29	51.24	12.47	
						(Ca,Mg)SiO ₃ (**)	14.87	49.52	15.03	20.57	
4	5.00	62.70	22.80	9.50		Matrix	5.58	57.02	27.14	10.26	
						SiO ₂	0.00	100.00	0.00	0.00	
5	5.00	62.70	30.40	1.90		Matrix	5.95	56.36	35.54	2.15	
						SiO ₂	0.00	100.00	0.00	0.00	
6	5.00	57.00	28.50	9.50							
7	5.00	49.03	34.89	11.09		Matrix	8.40	54.53	29.83	7.23	
						Ca ₂ MgSi ₂ O ₇	0.34	44.09	41.22	14.35	
8	5.00	46.30	22.86	25.83		Mg ₂ SiO ₄	0.00	43.10	1.83	55.07	
						(Ca,Mg)SiO ₃ (**)	6.58	48.91	32.66	11.85	
9	5.00	37.80	38.70	13.50	5.00	Matrix	5.88	41.91	35.11	5.44	11.67
						Ce ₂ O ₃	98.89	0.00	1.11	0.00	0.00
						CaMgSiO ₄	0.22	38.64	35.30	25.83	0.00
						Ca ₃ MgSi ₂ O ₈	1.35	36.57	49.98	12.10	0.00
10	2.00	39.06	39.99	13.95	5.00	(Ca,Mg,Ce)(Al,Mg)(Al,Si) ₂ O ₆ (*)	20.86	36.15	16.47	10.18	16.35
						Mg ₂ SiO ₄	0.00	42.46	3.37	54.17	0.00
						Ca ₂ MgSi ₂ O ₇	0.00	42.22	41.01	13.42	3.36
						Ca ₃ MgSi ₂ O ₈	0.00	36.45	51.13	12.41	0.00
11	1.00	39.48	40.42	14.10	5.00	Ca ₃ MgSi ₂ O ₈	0.00	36.19	51.35	12.47	0.00
						CaMgSiO ₄	0.00	38.26	35.34	26.40	0.00
						Matrix	1.72	43.39	36.33	10.24	8.33
12	5.00	37.80	38.70	13.50	5.00	Matrix	5.79	50.41	24.29	6.48	13.03
						Ce ₂ O ₃	100.00	0.00	0.00	0.00	0.00
						CaMgSiO ₄	0.00	38.29	36.60	25.11	0.00
						Ca ₃ MgSi ₂ O ₈	0.00	36.39	51.66	11.95	0.00

Slag sample	Initial composition (wt.-%)					Phase	Final composition (wt.-%)				
	Ce ₂ O ₃	SiO ₂	CaO	MgO	Al ₂ O ₃		Ce ₂ O ₃	SiO ₂	CaO	MgO	Al ₂ O ₃
13	2.00	39.06	39.99	13.95	5.00	Matrix	3.95	44.14	36.36	5.43	10.12
						CaMgSiO ₄	0.00	38.48	35.32	26.20	0.00
						Ca ₃ MgSi ₂ O ₈	0.00	36.78	51.21	12.01	0.00
14	2.00	58.80	29.40	9.80	Matrix	2.46	59.31	28.43	9.79		
15	1.00	59.40	29.70	9.90	Matrix	1.03	60.43	29.95	8.59		
16	1.00	41.58	42.57	14.85	CaMgSiO ₄	0.00	37.90	36.91	25.18		
					Ca ₃ MgSi ₂ O ₈	0.00	35.54	52.79	11.67		
					(Ca,Mg)SiO ₃ (**)	1.95	47.13	44.20	6.72		

Note:

(*) Proposed formula

(**) inclusive dissolved Ce₂O₃

This chapter also shows microstructure images of the phases through SEM analysis. Figure 11 to Figure 26 illustrate microstructure of the slag samples after non-isothermal heat treatment.

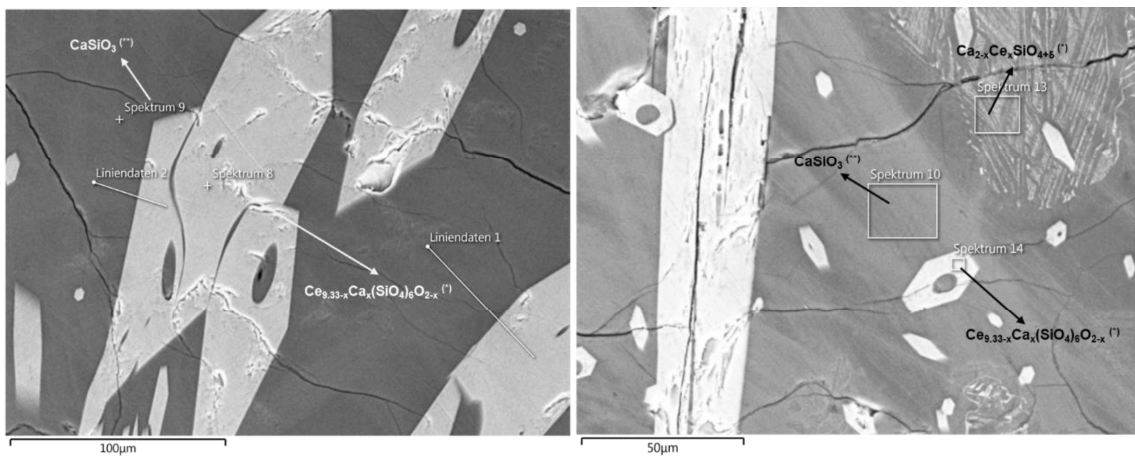


Figure 11. Microstructure of the slag sample 1 after non-isothermal heat treatment

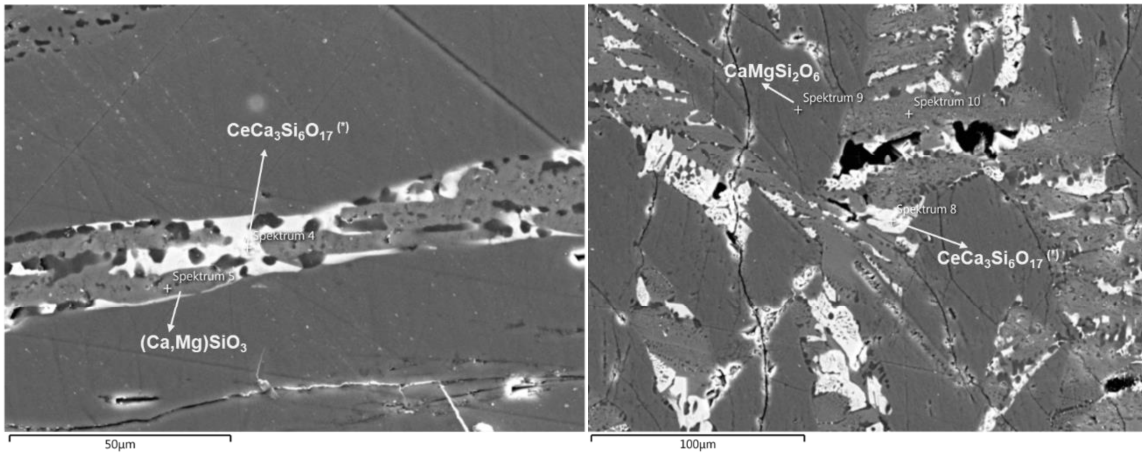


Figure 12. Microstructure of the slag sample 2 after non-isothermal heat treatment

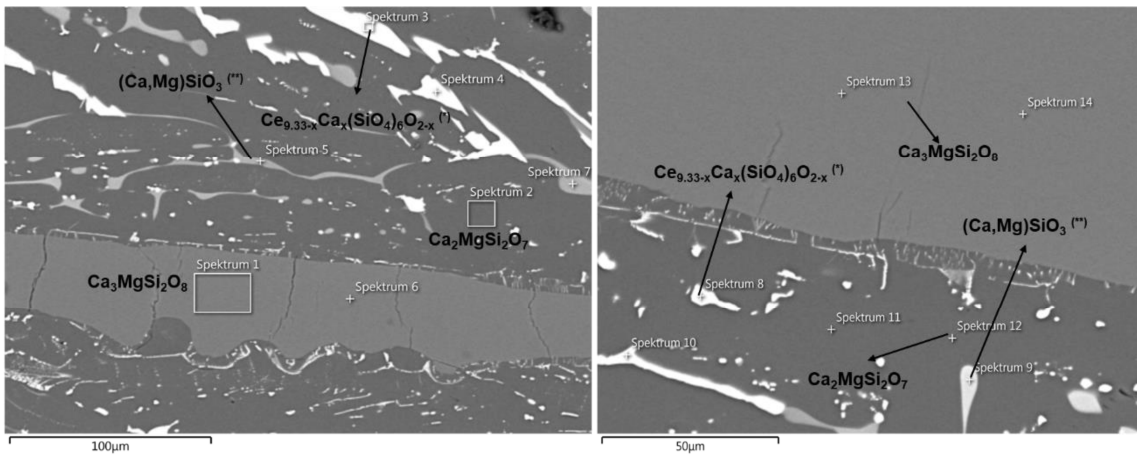


Figure 13. Microstructure of the slag sample 3 after non-isothermal heat treatment

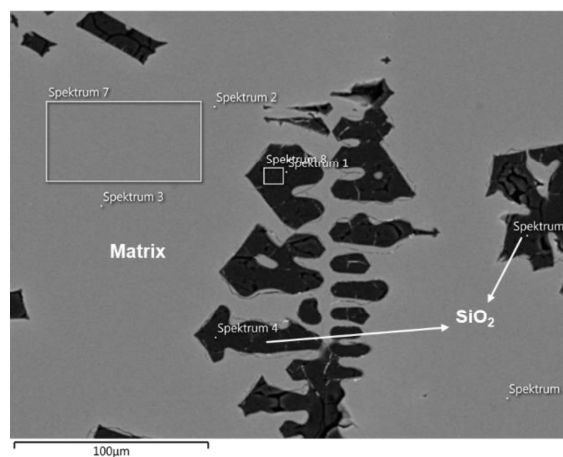


Figure 14. Microstructure of the slag sample 4 after non-isothermal heat treatment

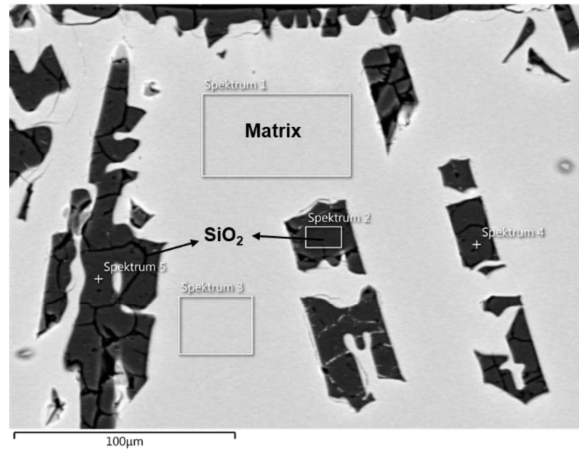


Figure 15. Microstructure of the slag sample 5 after non-isothermal heat treatment

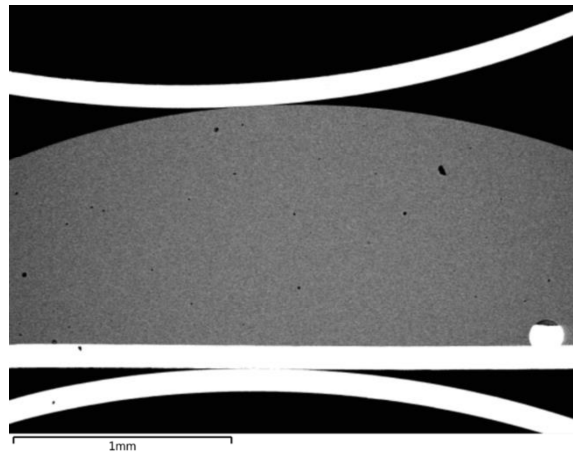


Figure 16. Microstructure of the slag sample 6 after non-isothermal heat treatment

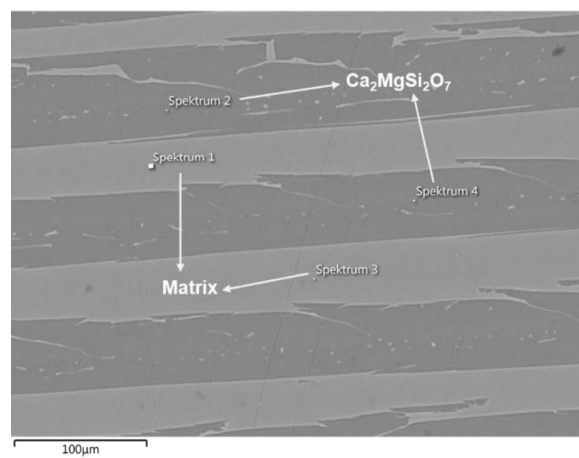


Figure 17. Microstructure of the slag sample 7 after non-isothermal heat treatment

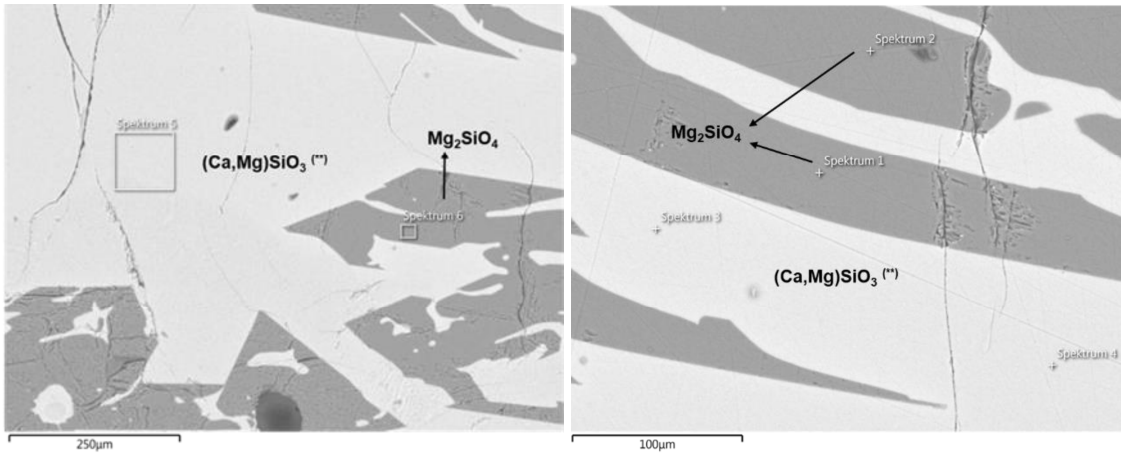


Figure 18. Microstructure of the slag sample 8 after non-isothermal heat treatment

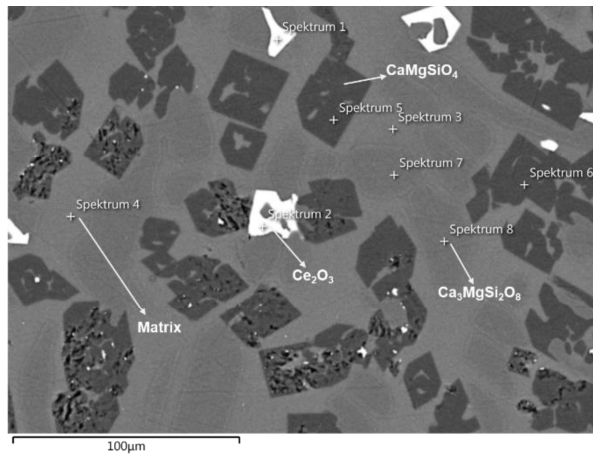


Figure 19. Microstructure of the slag sample 9 after non-isothermal heat treatment

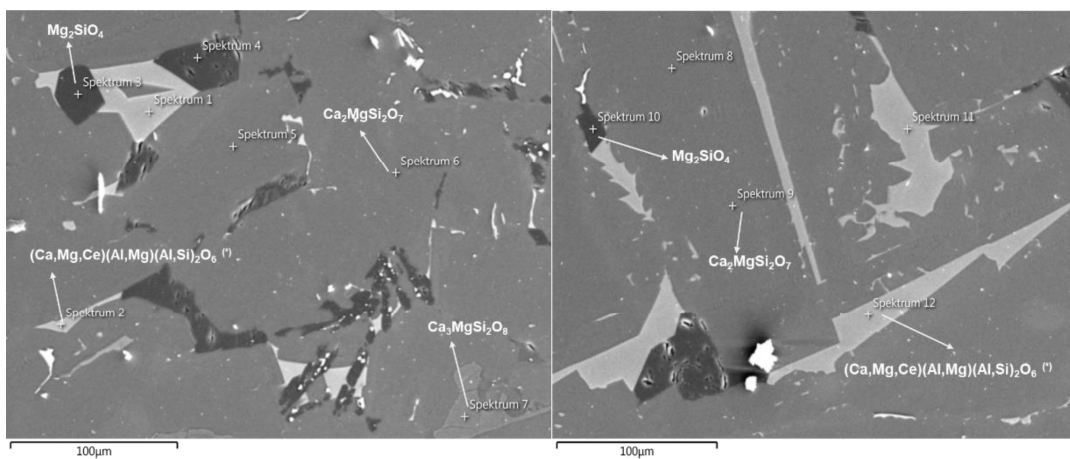


Figure 20. Microstructure of the slag sample 10 after non-isothermal heat treatment

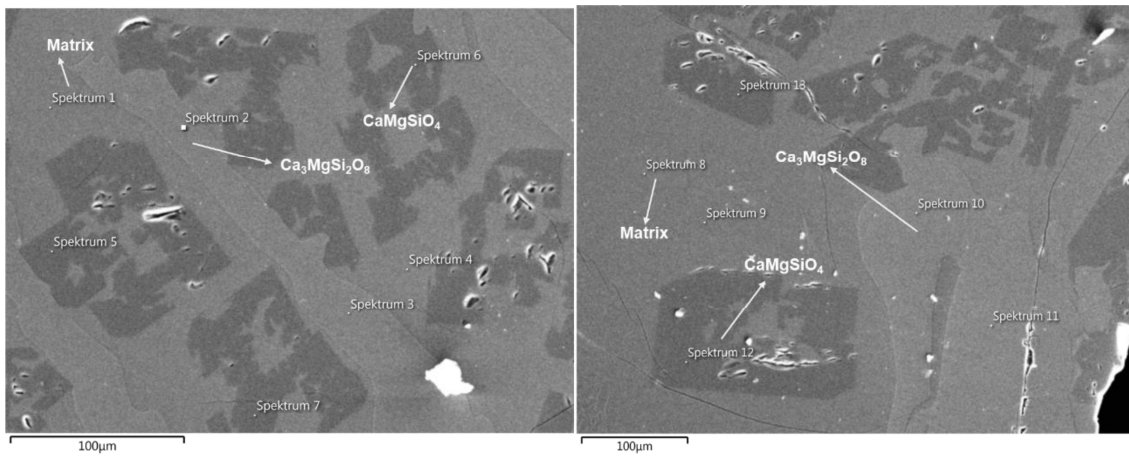


Figure 21. Microstructure of the slag sample 11 after non-isothermal heat treatment

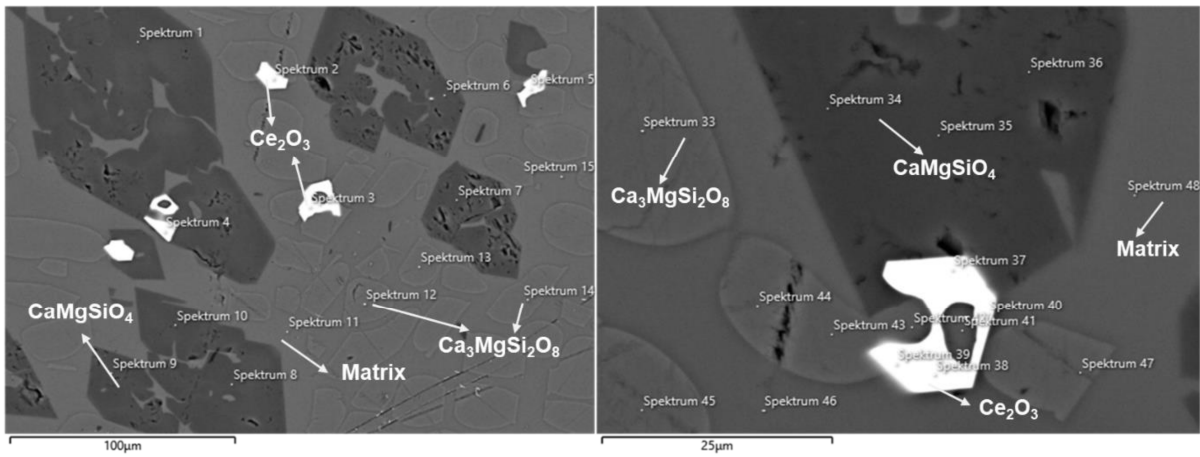


Figure 22. Microstructure of the slag sample 12 after non-isothermal heat treatment

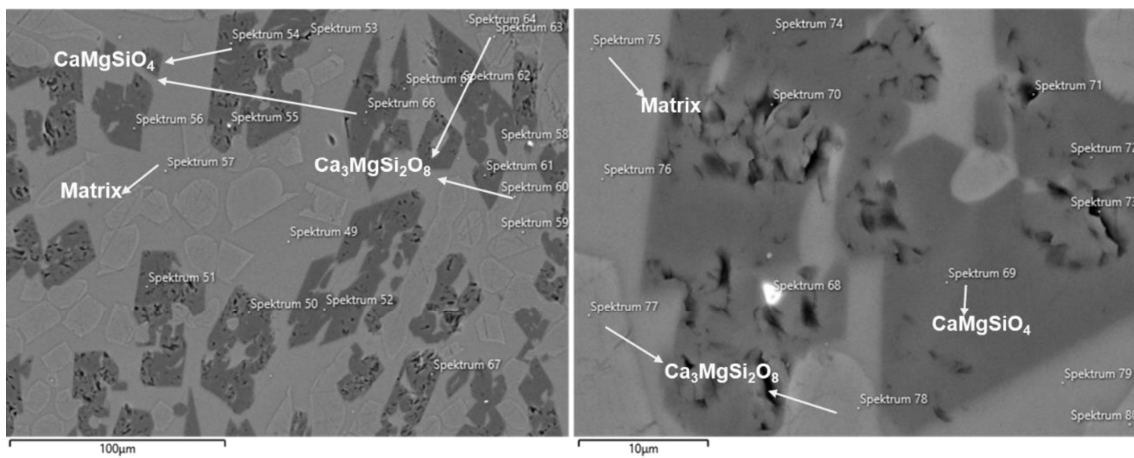


Figure 23. Microstructure of the slag sample 13 after non-isothermal heat treatment

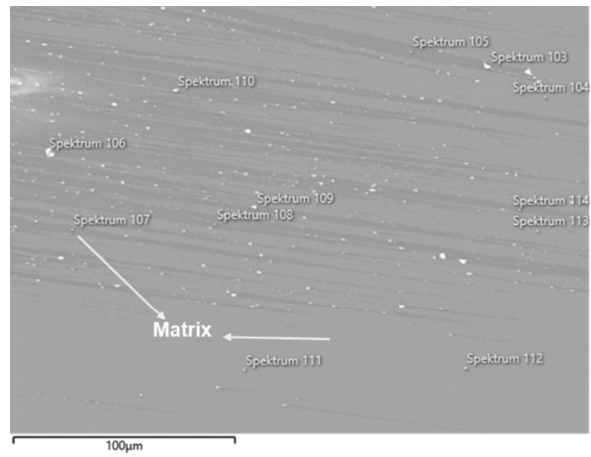


Figure 24. Microstructure of the slag sample 14 after non-isothermal heat treatment

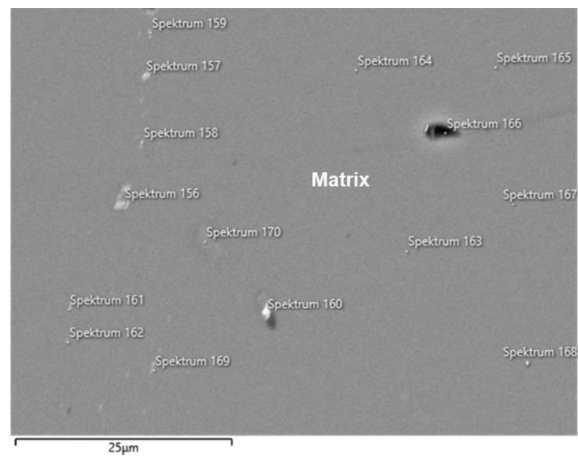


Figure 25. Microstructure of the slag sample 15 after non-isothermal heat treatment

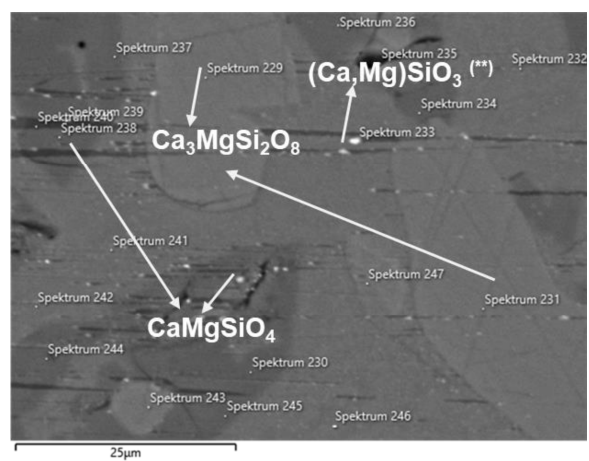


Figure 26. Microstructure of the slag sample 16 after non-isothermal heat treatment

5 Discussion

This chapter discusses further analysis of the possibility of Ce-incorporating phase formation for each slag sample. The morphology and compositions of the phases are discussed based on the data from SEM-EDS analyses for each slag sample summarized in Table 4 as well as Figure 11 to Figure 26. The detailed compositions of the phases for each sample retrieved from EDS analysis are given in Appendix B. This chapter also discusses the effect of CeO₂ content, ratio of CaO/MgO, presence of aluminum oxide as well as melting time during the heat treatment process on several generated phases.

5.1 Experiment Result of Slag Sample 1 after Non-isothermal Treatment at 1550 °C for Melting Time of 1 Hour

This experiment investigated a possibility for the generation of cerium-incorporating phases in the system CaO-SiO₂-Ce₂O₃. The respective composition of CaO, SiO₂, and CeO₂ used in the slag sample 1 were 15 wt.-%, 40 wt.-%, and 45 wt.-%. These compounds were mixed and then melted at 1550 °C for 1 hour. The SEM and EDS analyses (Figure 11) verified after the cooling process the existence of two phases, namely CaSiO₃ and Ce_{9.33-x}Ca_x(SiO₄)₆O_{2-x}. The latter incorporates a higher cerium content than the region of spectrum 13, which includes at least two different phases according to its striped appearance. As illustrated by Figure 11, the region of spectrum 13 contains 11.4 wt.-% Ce₂O₃, whereas the phase Ce_{9.33-x}Ca_x(SiO₄)₆O_{2-x} of spectrum 14 comprises a much higher Ce₂O₃ content of 49.2 wt.-%. These data have been normalized by converting compositions of each element in the sample from EDS analysis into their oxides. Ca_{2-x}Ce_xSiO_{4+δ} originated from Ca₂SiO₄ as parental compound by substituting Ce³⁺ for a part of Ca²⁺ [24]. In contrast, Ce_{9.33-x}Ca_x(SiO₄)₆O_{2-x} was formed through replacing partially Ce³⁺ in the parental compound Ce_{9.33}(SiO₄)₆O₂ by Ca²⁺ [24]. This phase has hexagonal form as RE crystal has sufficient time to growth.

5.2 Experiment Results of Slag Samples with Fixed Composition of CeO₂ and Varied Composition of CaO, MgO, and SiO₂ for Melting Time of 15 minutes

The experiments were carried out to investigate the distribution of cerium oxide to different phases in the system CaO-MgO-SiO₂ for six different slag compositions represented by point A to F in Figure 5. Ratio of CaO/MgO and basicity for each point were different. The content of CeO₂ used in these experiments was a constant 5 wt.-% while other oxides compositions were adjusted depending on the selected points. The detailed compositions of samples used are given in Table 5. They were melted for 15 minutes at 1600 °C except slag sample 2 which was melted at 1400 °C.

Table 5. The detailed compositions of samples used within the region of liquidus temperatures below 1500 °C for the system CaO-MgO-SiO₂

Slag Sample	Test Point	Initial Composition (wt.-%)				Ratio CaO/MgO	Basicity
		CeO ₂	SiO ₂	CaO	MgO		
2	C	5	57	29	10	3.00	0.67
3	A	5	40	41	14	2.87	1.38
4	D	5	63	23	10	2.40	0.52
5	E	5	63	30	2	16.00	0.52
6	C	5	57	29	10	3.00	0.67
7	B	5	49	35	11	3.15	0.94
8	F	5	46	23	26	0.89	1.05

As shown in Table 4, there were 3 phases generated after slag sample 2 were melted at 1400 °C for 15 minutes. An Ce-incorporating phase was found which composition fits the proposed compound CeCa₃Si₆O₁₇ containing about 35 wt.-% Ce₂O₃. The other two phases appear as (Ca,Mg)SiO₃ and CaMgSi₂O₆ as illustrated in Figure 12. The SEM result showed that the Ce-incorporating phase has no specific form, instead cerium was distributed in white area as represented by spectrums 4 and 8. (Ca,Mg)SiO₃ containing low magnesium exists around the Ce-incorporating phase with a light grey color as represented by spectrum 5. Spectrum 9 represents CaMgSi₂O₆. As reported by [57], four phases can be found in the ternary system CaO-MgO-SiO₂, namely diopside (CaMgSi₂O₆), akermanite (Ca₂MgSi₂O₇), merwinite (Ca₃MgSi₂O₈), and monticellite (CaMgSiO₄). Diopside phase can be generated when $X_{MgO}/(X_{CaO}+X_{MgO}) = 0.5$ at 1400 °C. Therefore, CaMgSi₂O₆ is a stable phase in this experiment.

When the temperature was increased to 1600 °C, no result was obtained from the experiment. The melted slag sample 6 was transparent; thus, no partitioning of the sample into several phases could be detected through EDS analysis. From SEM observation as shown in

Figure 16, it was found that the melted slag sample was constituted of a single homogeneous phase. Two experiments with the same condition were carried out but still produced the same results. Therefore, no separation into several different phases could be observed at these experimental parameters.

The next experiment was carried out at test point A with the other parameters were maintained as before. The basicity in this point was the highest of all selected in this region. Figure 13 shows the results of slag sample 3 consisting of four different phases. $\text{Ca}_2\text{MgSi}_2\text{O}_7$ and merwinite phase ($\text{Ca}_3\text{MgSi}_2\text{O}_8$) were found as represented by spectrums 12 and 13, respectively. Based on SEM-EDS analysis, cerium was incorporated in two different phases, namely $\text{Ce}_{9.33-x}\text{Ca}_x(\text{SiO}_4)_6\text{O}_{2-x}$ phase represented by spectrum 8 and $(\text{Ca},\text{Mg})\text{SiO}_3$ with dissolved Ce_2O_3 represented by spectrum 9. The $\text{Ce}_{9.33-x}\text{Ca}_x(\text{SiO}_4)_6\text{O}_{2-x}$ phase of this experiment had similar composition with that of slag sample 1 but did not have a certain specific form. Compared to previous experiment, it can be seen that basicity affects crystallization behavior of RE-incorporating phase through producing different geometries of crystalline phases.

The next experiments were carried out at points D and E in Figure 5. Slag sample 4 representing test point D and slag sample 5 representing test point E have the same basicity of 0.52 but different CaO/MgO ratios of 2.40 and 16.00, respectively. Due to the high content of SiO_2 used in these experiments, it is likely to be formed again as shown in Figure 14 and Figure 15, respectively. Whereas cerium oxide remained in the matrix for both experiments. At low basicity, high content of SiO_2 in slag leads to high slag viscosity and inferior slag fluidity thus increases the obstruction of crystal growth [39].

Since cerium oxide was found in Ce-incorporating phases at point A and C, it was interesting to observe a particular composition in the middle of those points. This point was labelled as point B in Figure 5. The respective slag sample 7 with a basicity of 0.94 were melted at $1600\text{ }^\circ\text{C}$ for 15 minutes. Figure 17 shows that cerium oxide was mainly found in the matrix and only to a small content in $\text{Ca}_2\text{MgSi}_2\text{O}_7$. The latter generated in the experiment was identified as akermanite ($\text{Ca}_2\text{MgSi}_2\text{O}_7$) based on EDS analysis.

The last point observed was Point F in Figure 5. Slag sample 8 comprises the lowest CaO/MgO ratio of 0.89 and a basicity of 1.05 and was melted at $1600\text{ }^\circ\text{C}$ for 15 minutes. After cooling process, 2 different areas can be distinguished as shown in Figure 18, namely matrix and an olivine phase (Mg_2SiO_4). The first contains about 7 wt.-% Ce_2O_3 and a high SiO_2 content of nearly 50 wt.-% and corresponds therefore to $(\text{Ca},\text{Mg})\text{SiO}_3$ with dissolved Ce_2O_3 . The olivine phase generated in the experiment contains only 1.83 wt.-% CaO. Since $X_{\text{MgO}}/X_{\text{MgO}}+X_{\text{CaO}} = 0.98$, therefore it could be assumed that forsterite phase was generated. Forsterite represents Mg_2SiO_4 -rich olivine [58].

5.3 Experiment Results of Slag Samples with the Presence of Al₂O₃

The following subchapters discuss the result of non-isothermal treatment of slag samples which contain 5 wt.-% Al₂O₃ in addition. The concentration of CeO₂ used in the experiments was varied between 5 wt.-%, 2 wt.-%, and 1 wt.-%. Also, the melting times of 15 minutes or 1 hour were applied in order to observe the effect of melting time on crystallization behavior. The experimental parameters used in the experiments were same for slag sample 3 that resulted in two different Ce-incorporating phases.

5.3.1 Experiment Results of Slag Samples with Additionally Containing Al₂O₃ with Varied Concentrations of CeO₂ at 1600 °C for a Melting Time of 15 Minutes

The experiment using slag sample 9 with 5 wt.-% CeO₂ and 5 wt.-% Al₂O₃ produced regions with four different compositions, namely matrix, Ce₂O₃, Ca₃MgSi₂O₈ (merwinite), and CaMgSiO₄ (monticellite). Based on Table 4, cerium was found in matrix and cerium oxide. Since Ce₂O₃ is an unstable phase, the Ce in Ce₂O₃ can be easily oxidized to the CeO₂ again during the quenching process [24]. Therefore, it could be concluded that cerium was remained in form of its initial particles rather than being incorporated in the identified silicate or dissolved in the matrix phases. As illustrated in Figure 19, the merwinite phase was represented by spectrum 8 with a dark grey color. It is arguable that merwinite cannot exist in the experiment as its melting temperature (1575 °C) is lower than the process temperature (1600°C). Merwinite melts incongruently to form Ca₂SiO₄, MgO, and liquid. Since this study was not focused on the temperature at which the phase started to form, the mechanism of merwinite formation was difficult to determine. Based on EDS analysis on spectrum 8, the phase has molar Mg/(Ca+Mg) ratio of 0.25 which corresponds to stoichiometric merwinite and the (Ca+Mg)/Si ratio of 1.96 which is approximately equal to 2 indicating that merwinite solution exists [58]. The existence of this phase in the sample can be explained either the temperature of the sample did not reach the melting temperature of that solid solution or it originated during cooling down the sample after the experiment.

When CeO₂ content was decreased to 2 wt.-% as in slag sample 10, there were four phases generated during the heat treatment process. These phases comprise Ca₂MgSi₂O₇, Mg₂SiO₄, Ca₃MgSi₂O₈, and (Ca,Mg,Ce)(Al,Mg)(Al,Si)₂O₆ as shown in Figure 20. In Mg₂SiO₄ phase, CaO existed in a low content, thus a Mg-rich olivine phase was likely generated in this composition. Similar to previous experiment, Ca₃MgSi₂O₈ was found in this experiment, but its presence

was low as represented in spectrum 7 in Figure 20. In the slag dominated by CaO, MgO, Al₂O₃, and SiO₂, cerium was incorporated in pyroxene-like phase which has general formula of (Y)(X)(Al,Si)₂O₆ with Y being Ca²⁺, Mg²⁺, REE³⁺, and X being Mg²⁺, Al³⁺. In this phase, about 40-50 wt.-% of CaO are replaced by REEs as the ionic radii and the oxygen coordination of Ca²⁺ and REE³⁺ are quite similar [59], [60]. Consequently, Ca can be exchanged by cerium in pyroxene-like phases.

When a further decrease of 1 wt.-% CeO₂ was used in slag sample 11, three distinguishable regions were generated in the experiment. These consist of matrix, CaMgSiO₄, and Ca₃MgSi₂O₈. The matrix contains around 2 wt.-% Ce₂O₃ and 8 wt.-% Al₂O₃. Unlike the previous experiments, there was no specific Ce-incorporating phase found in this composition as shown in Figure 21. This may be due to the CeO₂ content used in the slag was too low, only 1 wt.-% so it is not sufficient to form a Ce-incorporating phase with other elements.

5.3.2 Experiment Results of Slag Samples with Additionally Containing Al₂O₃ with Varied Compositions of CeO₂ at 1600 °C for a Melting Time of 1 Hour

In the experiment using a CeO₂ content of 5 wt.-%, there were no changes of generated phases even the melting time was increased to 1 hour. The microstructure of slag sample 12 from this experiment (Figure 22) shows a similar microstructure as the sample 9 melted for 15 minutes (Figure 19). There were four distinguishable regions generated, namely matrix, Ce₂O₃, CaMgSiO₄, and Ca₃MgSi₂O₈. Based on Table 4, Al₂O₃ was only found in matrix and not detected in other regions through EDS analysis. Ce₂O₃ still remained in this treatment, but as mentioned above, the phase was unstable so could not be considered as Ce-incorporating phase for the process of RE-bearing slag.

The next experiment was to reduce the CeO₂ content in slag sample 13 to 2 wt.-%. Figure 23 illustrated the microstructure of the slag sample after melting for 1 hour. Matrix and merwinite (Ca₃MgSi₂O₈) were found as in slag sample 10. However, cerium exists here together with other components to form a particular phase which was suspected to be Ce₂CaMgSi₂O₉. This phase contained 63.76 wt.-% Ce₂O₃ according to the measurement. Anyhow, due to the very small particle size, it has to be assumed that part of the surrounding area was also measured and consequently, also this particle exhibits an undissolved initial particle of cerium oxide.

5.4 Experiment Results of Slag Samples with Varied Composition of CeO₂ for Melting Time of 1 hour without the Presence of Al₂O₃

After studying the effect of Al₂O₃ and an increase of the melting time for slag samples with certain compositions of CeO₂, CaO, MgO, and SiO₂, the next parameter tested was to vary the CeO₂ content of slag samples containing no Al₂O₃ which were melted for 1 hour at 1600 °C. The slag samples 14 and 15 exhibited a CeO₂ content of 2 wt.-% and 1 wt.-%, respectively. The other oxides compositions of CaO, MgO, and SiO₂ were adjusted based on point C in Figure 5. The microstructure of slag sample 14 is shown in Figure 24, whereas the microstructure of slag sample 15 is shown in Figure 25. No discrete phases were identified in both melted slag samples, only matrix. Formation of a single phase is also reported by [54] on system CaO-SiO₂-Ce₂O₃. The slag sample with the parameters closest to these experiments was slag sample 6, which has oxides base composition at Point C and 5 wt.-% CeO₂. The slag sample was melted at 1600 °C with a lower time of 15 minutes, but it could not be analyzed as an amorphous phase emerged. Therefore, further study related to the parameters of slag samples 6, 14, and 15 was interested to conduct in aims to elucidate the phases formation mechanism.

The last experiment carried out was to change the content of CeO₂ to 1 wt.-% as represented by slag sample 16. Based on SEM-EDS analysis, there were three distinguishable regions from the treatment, namely matrix, CaMgSiO₄, and Ca₃MgSi₂O₈ as shown in Figure 26. The phases from this experiment were consistent with the phases produced from slag sample 11 which composed of 1 wt.-% CeO₂ and 5 wt.-% Al₂O₃ and was melted for 15 minutes. From these two samples, it could be concluded that the presence of Al₂O₃ and increase in melting time did not affect the crystallization behavior of phases for low content of 1 wt.-% CeO₂ as cerium oxide remained in the matrix.

5.5 Diagram of the System CaO-MgO-SiO₂-Ce₂O₃ at Room Temperature

According to composition of the phases shown in Table 4, the generated phases from the slag samples melted at various parameters were plotted on a ternary diagram (Figure 27) of the system CaO-MgO-SiO₂-Ce₂O₃.

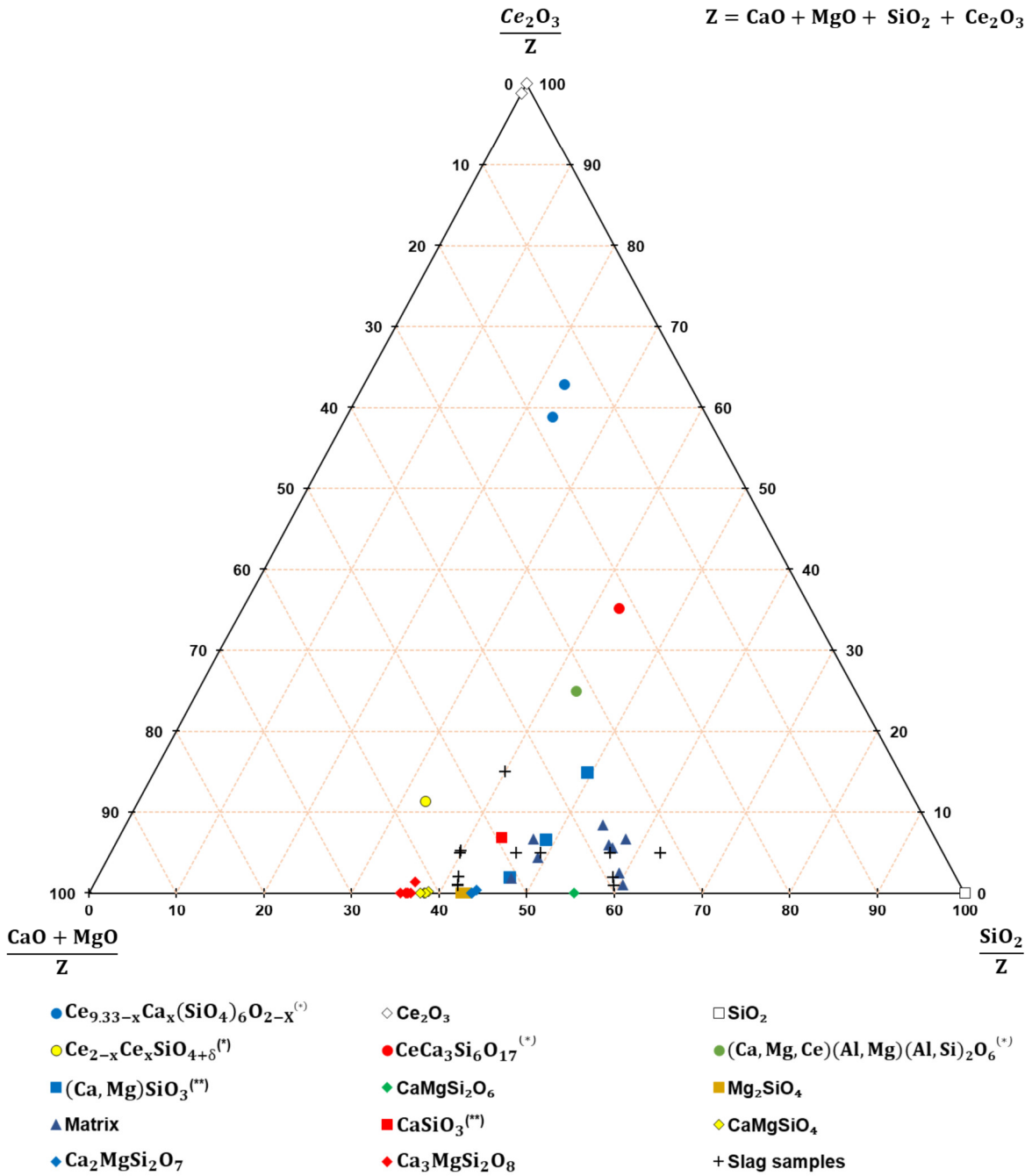


Figure 27. Diagram of the system CaO-MgO-SiO₂-Ce₂O₃ at room temperature with compositions of the slag samples

6 Conclusion

A series of experiments proves that a heat treatment process can be used to concentrate the REE content of slags in certain phases, while others remain free of them. Several conclusions can be derived from the non-isothermal heat treatment experiments carried out under different parameter conditions, as follows:

- 1) Cerium representing REEs in the experiments can be enhanced by forming a Ce-incorporating phase which is $\text{Ce}_{9.33-x}\text{Ca}_x(\text{SiO}_4)_6\text{O}_{2-x}$ containing about 59-63 wt.-% cerium oxide. It can also be found at a significantly lower content in some phases such as $\text{Ca}_{2-x}\text{Ce}_x\text{SiO}_{4+6}$, CaSiO_3 , $\text{CeCa}_3\text{Si}_6\text{O}_{17}$, $(\text{Ca},\text{Mg})\text{SiO}_3$, and $\text{Ce}_2\text{Ca}_4\text{Mg}_4\text{Al}_4\text{Si}_9\text{O}_{35}$.
- 2) The other phases observed in the experiments are wollastonite (CaSiO_3), diopside ($\text{CaMgSi}_2\text{O}_6$), akermanite ($\text{Ca}_2\text{MgSi}_2\text{O}_7$), merwinite ($\text{Ca}_3\text{MgSi}_2\text{O}_8$), and monticellite (CaMgSiO_4).
- 3) In the system CaO-MgO-SiO_2 with an initial cerium oxide content of 5 wt.-%, the highest cerium oxide concentration in Ce-incorporating phase, $\text{Ce}_{9.33-x}\text{Ca}_x(\text{SiO}_4)_6\text{O}_{2-x}$, reached about 63 wt.-% which is obtained from the experiment carried out at 1600 °C for 15 minutes with the basicity of 1.38 (test point A in Figure 5).
- 4) Under the same parameter conditions, no separation into several phases can be observed from the experiment carried out at basicity of 0.67 (test point C) as a single homogenous phase resulted. When the basicity is reduced to 0.52 (test point D and E), the generated phases are dominated by SiO_2 due to its high content of the initial composition while cerium remains in matrix.
- 5) A matrix also originated from the experiments carried out at test Point C for a longer melting time (1 hour) with the respective CeO_2 contents in initial compositions of 2 wt.-% and 1 wt.-%.
- 6) When Al_2O_3 is added with a fixed content, cerium can be either incorporated in a certain phase such as $(\text{Ca},\text{Mg},\text{Ce})(\text{Al},\text{Mg})(\text{Al},\text{Si})_2\text{O}_6$ (21 wt.-% Ce) or remained in the matrix (1.7-5.8 wt.-% Ce_2O_3). Despite, Ce_2O_3 appeared during the observation but cannot be considered as Ce-incorporating phase because the phase is unstable and likely represent incomplete dissolved CeO_2 particles of the initial powder mixture. Under these parameter conditions, the various initial compositions of Ce and melting times have no significant effect as the content of Ce in the generated phases remain low.

7 Bibliography

- [1] S. M. Jowitt, T. T. Werner, Z. Weng, and G. M. Mudd, "Recycling of the rare earth elements," *Curr Opin Green Sustain Chem*, vol. 13, pp. 1–7, Oct. 2018, doi: 10.1016/J.COAGSC.2018.02.008.
- [2] B. C. McLellan, G. D. Corder, A. Golev, and S. H. Ali, "Sustainability of the Rare Earths Industry," *Procedia Environ Sci*, vol. 20, pp. 280–287, Jan. 2014, doi: 10.1016/J.PROENV.2014.03.035.
- [3] K. Binnemans and P. T. Jones, "Rare Earths and the Balance Problem," *Journal of Sustainable Metallurgy*, vol. 1, no. 1, pp. 29–38, Mar. 2015, doi: 10.1007/s40831-014-0005-1.
- [4] I. B. de Lima and W. Leal Filho, *Rare earths industry: technological, economic, and environmental implications*.
- [5] L. M. Suli, W. H. W. Ibrahim, B. A. Aziz, M. R. Deraman, and N. A. Ismail, "A Review of Rare Earth Mineral Processing Technology," *Chemical Engineering Research Bulletin*, vol. 19, p. 20, 2017, doi: 10.3329/ceerb.v19i0.33773.
- [6] C. K. Krishnamurthy, Nagaiyar; Gupta, *Extractive Metallurgy of Rare Earths*, 2nd Edition. CRC Press, 2016.
- [7] K. Binnemans *et al.*, "Recycling of rare earths: a critical review," *J Clean Prod*, vol. 51, pp. 1–22, Jul. 2013, doi: 10.1016/J.JCLEPRO.2012.12.037.
- [8] J. Lucas, P. Lucas, T. Le Mercier, A. Rollat, and W. G. Davenport, *Rare Earths: Science, Technology, Production and Use*. Elsevier, 2015. doi: 10.1016/b978-008044029-3/50005-8.
- [9] D. Qi, *Hydrometallurgy of Rare Earths: Extraction and Separation*. India: Dennis, Susan, 2018. doi: 10.1016/c2016-0-05328-7.
- [10] J. Zhang, B. Zhao, and B. Schreiner, *Separation hydrometallurgy of rare earth elements*. 2016. doi: 10.1007/978-3-319-28235-0.
- [11] F. Vernilli, D. Camargo Vernilli, B. Ferreira, and G. Silva, "Characterization of a rare earth oxide obtained from xenotime mineral," *Mater Charact*, vol. 58, no. 1, pp. 1–7, 2007, doi: 10.1016/j.matchar.2006.01.022.
- [12] K. Binnemans, P. T. Jones, B. Blanpain, T. Van Gerven, and Y. Pontikes, "Towards zero-waste valorisation of rare-earth-containing industrial process residues: a critical review," *J Clean Prod*, vol. 99, pp. 17–38, Jul. 2015, doi: 10.1016/J.JCLEPRO.2015.02.089.

- [13] N. Swain and S. Mishra, "A review on the recovery and separation of rare earths and transition metals from secondary resources," *J Clean Prod*, vol. 220, pp. 884–898, 2019, doi: 10.1016/j.jclepro.2019.02.094.
- [14] A. Kumari, R. Panda, J. Rajesh Kumar, K. Yoo, and J. Y. Lee, "Review on hydrometallurgical recovery of rare earth metals," *Hydrometallurgy*, vol. 165, pp. 2–26, Oct. 2016, doi: 10.1016/J.HYDROMET.2016.01.035.
- [15] C.-J. Kim *et al.*, "Leaching kinetics of lanthanum in sulfuric acid from rare earth element (REE) slag," *Hydrometallurgy*, vol. 146, pp. 133–137, May 2014, doi: 10.1016/J.HYDROMET.2014.04.003.
- [16] T. Jun, Y. Jingqun, C. Ruan, R. Guohua, J. Mintao, and O. Kexian, "Kinetics on leaching rare earth from the weathered crust elution-deposited rare earth ores with ammonium sulfate solution," *Hydrometallurgy*, vol. 101, no. 3–4, pp. 166–170, Mar. 2010, doi: 10.1016/J.HYDROMET.2010.01.001.
- [17] D. J. Sapsford, R. J. Howell, J. N. Geroni, K. M. Penman, and M. Dey, "Factors influencing the release rate of uranium, thorium, yttrium and rare earth elements from a low grade ore," *Miner Eng*, vol. 39, pp. 165–172, Dec. 2012, doi: 10.1016/J.MINENG.2012.08.002.
- [18] M. Kul, Y. Topkaya, and İ. Karakaya, "Rare earth double sulfates from pre-concentrated bastnasite," *Hydrometallurgy*, vol. 93, no. 3–4, pp. 129–135, Aug. 2008, doi: 10.1016/J.HYDROMET.2007.11.008.
- [19] A. T. Kandil, M. M. Aly, E. M. Moussa, A. M. Kamel, M. M. Gouda, and M. N. Kouraim, "Column leaching of lanthanides from Abu Tartur phosphate ore with kinetic study," *Journal of Rare Earths*, vol. 28, no. 4, pp. 576–580, Aug. 2010, doi: 10.1016/S1002-0721(09)60157-5.
- [20] G. A. Moldoveanu and V. G. Papangelakis, "Recovery of rare earth elements adsorbed on clay minerals: I. Desorption mechanism," *Hydrometallurgy*, vol. 117–118, pp. 71–78, Apr. 2012, doi: 10.1016/J.HYDROMET.2012.02.007.
- [21] Y. A. El-Nadi, "Lanthanum and neodymium from Egyptian monazite: Synergistic extractive separation using organophosphorus reagents," *Hydrometallurgy*, vol. 119–120, pp. 23–29, May 2012, doi: 10.1016/j.hydromet.2012.03.003.
- [22] D. Durinck *et al.*, "Hot stage processing of metallurgical slags," *Resour Conserv Recycl*, vol. 52, no. 10, pp. 1121–1131, 2008, doi: <https://doi.org/10.1016/j.resconrec.2008.07.001>.

- [23] Y. Liang, Y. Liu, R. Lin, D. Guo, and C. Liao, "Leaching of rare earth elements from waste lamp phosphor mixtures by reduced alkali fusion followed by acid leaching," *Hydrometallurgy*, vol. 163, pp. 99–103, 2016, doi: <https://doi.org/10.1016/j.hydromet.2016.03.020>.
- [24] X. Lan, J. Gao, Y. Du, and Z. Guo, "Thermodynamics and crystallization kinetics of REEs in CaO–SiO₂–Ce₂O₃ system," *Journal of the American Ceramic Society*, vol. 103, no. 4, pp. 2845–2858, 2020, doi: 10.1111/jace.16946.
- [25] W. Zhi *et al.*, "Phase equilibria of CaO–SiO₂–Gd₂O₃ system and the feasibility of rare-earth recovery," *Ceram Int*, vol. 44, no. 13, pp. 15896–15904, Sep. 2018, doi: 10.1016/J.CERAMINT.2018.06.006.
- [26] K. Binnemans, Y. Pontikes, P. Jones, T. Van Gerven, and B. Blanpain, "Recovery of rare earths from industrial waste residues: a concise review," in *3rd International Slag Valorisation Symposium*, Mar. 2013, pp. 191–205.
- [27] J. Li, X. He, and X. Zeng, "Designing and examining e-waste recycling process: methodology and case studies," *Environmental Technology (United Kingdom)*, vol. 38, no. 6, pp. 652–660, 2017, doi: 10.1080/09593330.2016.1207711.
- [28] M. Tanaka, T. Oki, K. Koyama, H. Narita, and T. Oishi, "Recycling of Rare Earths from Scrap," *Handbook on the Physics and Chemistry of Rare Earths*, vol. 43, pp. 159–211, Jan. 2013, doi: 10.1016/B978-0-444-59536-2.00002-7.
- [29] Y. Yang *et al.*, "REE Recovery from End-of-Life NdFeB Permanent Magnet Scrap: A Critical Review," *Journal of Sustainable Metallurgy*, vol. 3, no. 1, pp. 122–149, 2017, doi: 10.1007/s40831-016-0090-4.
- [30] S. T. Abrahami, Y. Xiao, and Y. Yang, "Rare-earth elements recovery from post-consumer hard-disc drives," *Mineral Processing and Extractive Metallurgy*, vol. 124, no. 2, pp. 106–115, 2015, doi: 10.1179/1743285514y.0000000084.
- [31] R. J. Weber and D. J. Reisman, "Rare Earth Elements: A Review of Production, Processing, Recycling, and Associated Environmental Issues," U.S. Environmental Protection Agency, Washington, DC, 2012.
- [32] H. Shen and E. Forssberg, "An overview of recovery of metals from slags," *Waste Management*, vol. 23, no. 10, pp. 933–949, Jan. 2003, doi: 10.1016/S0956-053X(02)00164-2.
- [33] I. Gaballah and E. Allain, "Recycling of strategic metals from industrial slag by a hydro- and pyrometallurgical process," *Resour Conserv Recycl*, vol. 10, no. 1–2, pp. 75–85, Apr. 1994, doi: 10.1016/0921-3449(94)90040-X.

- [34] Z. S. Abisheva *et al.*, “Recovery of rare earth metals as critical raw materials from phosphorus slag of long-term storage,” *Hydrometallurgy*, vol. 173, pp. 271–282, Nov. 2017, doi: 10.1016/J.HYDROMET.2017.08.022.
- [35] D. Cheret and S. Santen, “Battery recycling,” US 7169206B2, Jan. 20, 2007
- [36] M. Verhaeghe, F., Goubin, F., Yazicioglu, B., Schurmans, M., Thijs, B., Haesebroek, G. Tytgat, J., Van Camp, “Valorisation of Battery Recycling Slags,” *2nd International Slag Valorisation Symposium*, pp. 365–373, 2011.
- [37] J. Wang *et al.*, “Recovery of rare earths and aluminum from FCC waste slag by acid leaching and selective precipitation,” *Journal of Rare Earths*, vol. 35, no. 11, pp. 1141–1148, Nov. 2017, doi: 10.1016/J.JRE.2017.05.011.
- [38] X. Lan, J. Gao, Y. Li, and Z. Guo, “Thermodynamics and kinetics of REEs in CaO–SiO₂–CaF₂–Ce₂O₃ system: A theoretical basis toward sustainable utilization of REEs in REE-Bearing slag,” *Ceram Int*, vol. 47, no. 5, pp. 6130–6138, Mar. 2021, doi: 10.1016/J.CERAMINT.2020.10.192.
- [39] X. She, Z. An, Z. Zhang, T. Ma, and J. Wang, “Crystallization behavior of synthesized CaO–SiO₂–CaF₂–La₂O₃ rare earth-containing slag,” *ISIJ International*, vol. 60, no. 5, pp. 832–839, 2020, doi: 10.2355/isijinternational.ISIJINT-2019-557.
- [40] Ministry of Energy and Mineral Resources, “Kajian Potensi Mineral Ikutan Pada Pertambangan Timah,” 2017. Accessed: Jun. 19, 2023. [Online]. Available: <https://www.esdm.go.id/id/publikasi/publikasi-hasil-kajian>
- [41] W. Xin, Y. Deng, Y. Jiang, J. Zhang, and P. Wang, “Crystallization Characteristics of the CaO–SiO₂–Al₂O₃–La₂O₃ Rare Earth-Bearing Slag System,” *Transactions of the Indian Institute of Metals*, vol. 74, no. 6, pp. 1549–1556, Jun. 2021, doi: 10.1007/s12666-021-02246-1.
- [42] L. Liu, M. long Hu, C. guang Bai, X. wei Lü, Y. zhou Xu, and Q. yu Deng, “Effect of cooling rate on the crystallization behavior of perovskite in high titanium-bearing blast furnace slag,” *International Journal of Minerals, Metallurgy and Materials*, vol. 21, no. 11, pp. 1052–1061, Nov. 2014, doi: 10.1007/s12613-014-1009-3.
- [43] W. Yi, X. She, H. Zhang, Z. An, J. Wang, and Q. Xue, “Precipitation of Rare Earth Slag and the Crystallization Behavior of Rare Earth Phase,” *Metallurgical and Materials Transactions B: Process Metallurgy and Materials Processing Science*, vol. 52, no. 2, pp. 1095–1105, Apr. 2021, doi: 10.1007/s11663-021-02081-1.

- [44] R. De Carolis, D. Fontana, M. Pietrantonio, S. Pucciarmati, and G. N. Torelli, "A hydrometallurgical process for recovering rare earths and metals from spent fluorescent lamps," *Environ Eng Manag J*, vol. 14, no. 7, pp. 1603–1609, 2015.
- [45] C. Tunsu, M. Petranikova, C. Ekberg, and T. Retegan, "A hydrometallurgical process for the recovery of rare earth elements from fluorescent lamp waste fractions," *Sep Purif Technol*, vol. 161, pp. 172–186, 2016, doi: <https://doi.org/10.1016/j.seppur.2016.01.048>.
- [46] T. H. Le, A. Malfliet, B. Blanpain, and M. Guo, "Phase Relations of the CaO-SiO₂-Nd₂O₃ System and the Implication for Rare Earths Recycling," *Metallurgical and Materials Transactions B: Process Metallurgy and Materials Processing Science*, vol. 47, no. 3, pp. 1736–1744, 2016, doi: 10.1007/s11663-016-0634-9.
- [47] W. Zhi *et al.*, "Phase relations of CaO-Al₂O₃-Sc₂O₃ ternary system," *Journal of the American Ceramic Society*, vol. 102, no. 5, pp. 2863–2870, 2019, doi: 10.1111/jace.16104.
- [48] K. Tang *et al.*, "Recycling the rare earth elements from waste NiMH batteries and magnet scraps by pyrometallurgical processes," *Proceedings of the First International Symposium on Development of Rare Earths, Baotou, China*, no. July, pp. 8–12, 2014, doi: 10.13140/2.1.4500.6723.
- [49] T. Müller and B. Friedrich, "Development of a recycling process for nickel-metal hydride batteries," *J Power Sources*, vol. 158, no. 2, pp. 1498–1509, Aug. 2006, doi: 10.1016/J.JPOWSOUR.2005.10.046.
- [50] D.-G. Li, Q.-C. Bu, T.-P. Lou, and Z. Sui, "Morphology of Solidified Slag for RE₂O₃-CaO-SiO₂-CaF₂-MgO-Al₂O₃ System," *Journal of Iron and Steel Research*, vol. 16, pp. 30–33, 2004.
- [51] Y. Ding, J. Wang, G. Wang, and Q. Xue, "Innovative Methodology for Separating of Rare Earth and Iron from Bayan Obo Complex Iron Ore," *ISIJ International*, vol. 52, pp. 1772–1777, 2012, doi: 10.2355/isijinternational.52.1772.
- [52] X. Lan, J. Gao, Y. Li, and Z. Guo, "A green method of respectively recovering rare earths (Ce, La, Pr, Nd) from rare-earth tailings under super-gravity," *J Hazard Mater*, vol. 367, pp. 473–481, Apr. 2019, doi: 10.1016/J.JHAZMAT.2018.12.118.
- [53] D.-G. Li, J.-F. Wang, T.-P. Lou, and Z. Sui, "Precipitation kinetics of calcium cerite phase in slag bearing rare earths," *Journal of Iron and Steel Research*, vol. 16, pp. 64–67, 2004.

- [54] Z. Zhao, X. Chen, B. Glaser, and B. Yan, "Experimental Study on the Thermodynamics of the CaO-SiO₂-Ce₂O₃ System at 1873 K," *Metallurgical and Materials Transactions B: Process Metallurgy and Materials Processing Science*, vol. 50, no. 1, pp. 395–406, 2019, doi: 10.1007/s11663-018-1471-9.
- [55] J. Wang *et al.*, "Recovery of rare earths and aluminum from FCC catalysts manufacturing slag by stepwise leaching and selective precipitation," *J Environ Chem Eng*, vol. 5, no. 4, pp. 3711–3718, Aug. 2017, doi: 10.1016/J.JECE.2017.07.018.
- [56] Z. Karshigina, Z. Abisheva, Y. Bochevskaya, A. Akcil, and E. Sargelova, "Recovery of rare earth metals and precipitated silicon dioxide from phosphorus slag," *Miner Eng*, vol. 77, pp. 159–166, Jun. 2015, doi: 10.1016/J.MINENG.2015.03.013.
- [57] W. Huang, M. Hillert, and X. Wang, "Thermodynamic assessment of the CaO-MgO-SiO₂ system," *Metallurgical and Materials Transactions A*, vol. 26, no. 9, pp. 2293–2310, 1995, doi: 10.1007/BF02671244.
- [58] I.-H. Jung, S. A. Deckerov, and A. D. Pelton, "Critical thermodynamic evaluation and optimization of the CaO–MgO–SiO₂ system," *J Eur Ceram Soc*, vol. 25, no. 4, pp. 313–333, 2005, doi: <https://doi.org/10.1016/j.jeurceramsoc.2004.02.012>.
- [59] T. Elwert, D. Goldmann, T. Schirmer, and K. Strauß, "Affinity of rare earth elements to silico-phosphate phases in the system Al₂O₃-CaO-MgO-P₂O₅-SiO₂," *Chem Ing Tech*, vol. 86, no. 6, pp. 840–847, 2014, doi: 10.1002/cite.201300168.
- [60] "Mineralatlas Lexikon - Pyroxene group."
<https://www.mineralienatlas.de/lexikon/index.php/MineralData?mineral=Pyroxene+group> (accessed Jun. 19, 2023).

8 List of Figures

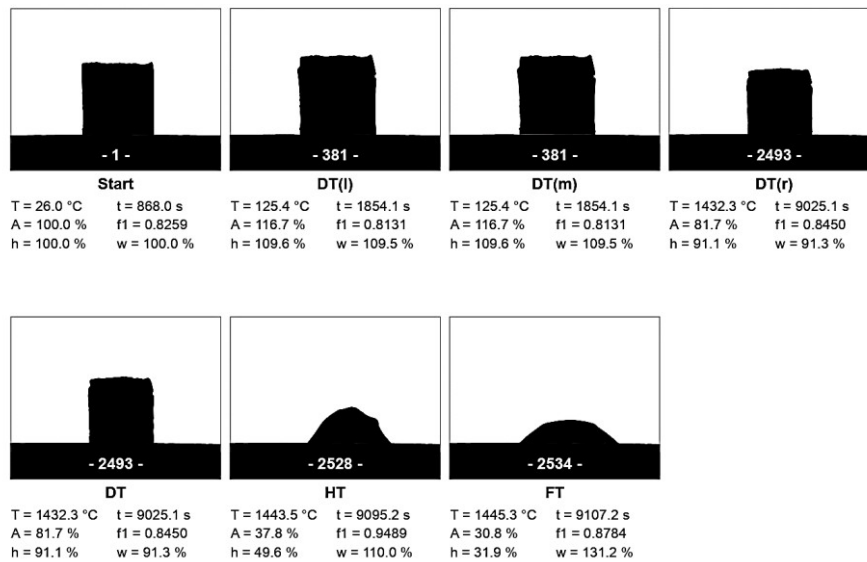
Figure 1.	The world's rare earth producing mines in 2013 [8]	2
Figure 2.	Recycling of REE-containing resources in many forms, revealing the importance of metal recovery from both flows and stocks of industrial process residues from primary and secondary metal production [3]	4
Figure 3.	Research methodology	7
Figure 4.	Schematic process of REE enrichment in slag through heat treatment process	12
Figure 5.	Ternary system of CaO-MgO-SiO ₂ at 1500 °C and 1 atm constructed using Factsage 8.0 in which an area with only liquid slag as stable phase was observed from which six test points were selected	13
Figure 6.	Flowchart of sequence of the test procedures	14
Figure 7.	Raw oxide materials used in the investigations, (a) calcium oxide, CaO; (b) magnesium oxide, MgO; (c) silicon dioxide, SiO ₂ ; (d) aluminum oxide, Al ₂ O ₃ ; and (e) cerium dioxide, CeO ₂	15
Figure 8.	Swing mill used in the preparation stage in order to obtain a homogenous slag feed	16
Figure 9.	Hot stage microscope used to observe melting behavior of slag samples	18
Figure 10.	Scanning Electron Microscope (SEM) equipped with an energy dispersive X-ray (EDS) detector used in the investigation	19
Figure 11.	Microstructure of the slag sample 1 after non-isothermal heat treatment.....	22
Figure 12.	Microstructure of the slag sample 2 after non-isothermal heat treatment.....	23
Figure 13.	Microstructure of the slag sample 3 after non-isothermal heat treatment.....	23
Figure 14.	Microstructure of the slag sample 4 after non-isothermal heat treatment.....	23
Figure 15.	Microstructure of the slag sample 5 after non-isothermal heat treatment.....	24
Figure 16.	Microstructure of the slag sample 6 after non-isothermal heat treatment.....	24
Figure 17.	Microstructure of the slag sample 7 after non-isothermal heat treatment.....	24
Figure 18.	Microstructure of the slag sample 8 after non-isothermal heat treatment.....	25
Figure 19.	Microstructure of the slag sample 9 after non-isothermal heat treatment.....	25
Figure 20.	Microstructure of the slag sample 10 after non-isothermal heat treatment.....	25
Figure 21.	Microstructure of the slag sample 11 after non-isothermal heat treatment.....	26
Figure 22.	Microstructure of the slag sample 12 after non-isothermal heat treatment.....	26
Figure 23.	Microstructure of the slag sample 13 after non-isothermal heat treatment.....	26
Figure 24.	Microstructure of the slag sample 14 after non-isothermal heat treatment.....	27
Figure 25.	Microstructure of the slag sample 15 after non-isothermal heat treatment.....	27
Figure 26.	Microstructure of the slag sample 16 after non-isothermal heat treatment.....	27
Figure 27.	Diagram of the system CaO-MgO-SiO ₂ -Ce ₂ O ₃ at room temperature with compositions of the slag samples.....	34

9 List of Tables

Table 1.	Distribution of REEs in many applications [4]	1
Table 2.	Potential sources of REEs recycling [1]	5
Table 3.	Initial compositions of slag samples and parameters of melting process	17
Table 4.	Compositions of phases in the quenched slag samples	21
Table 5.	The detailed compositions of samples used within the region of liquidus temperatures below 1500 °C for the system CaO-MgO-SiO ₂	29

10 Appendix

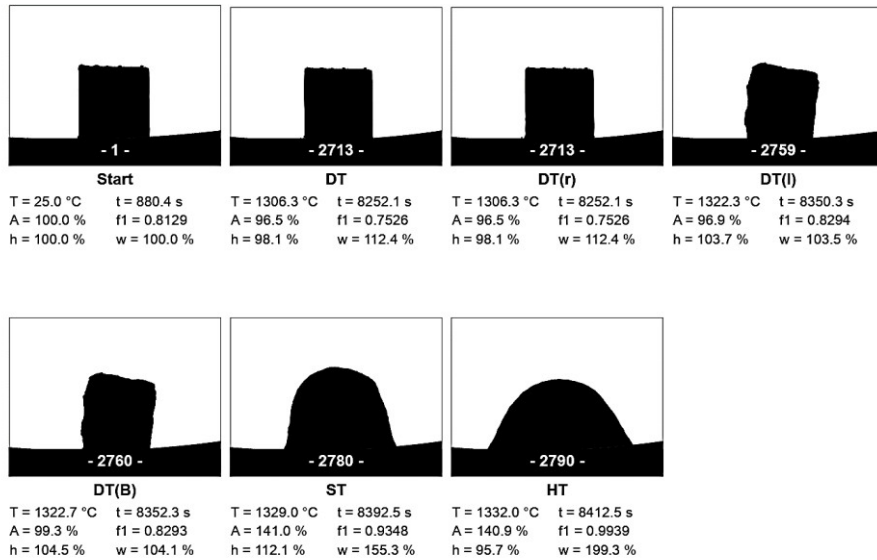
10.1 Appendix A – Data of Heat Treatment Process of the Slag Samples in Hot Stage Microscope



Legend

T	Temperature
t	Time
A	Area
f1	Aspect ratio 1
h	Height
w	Width

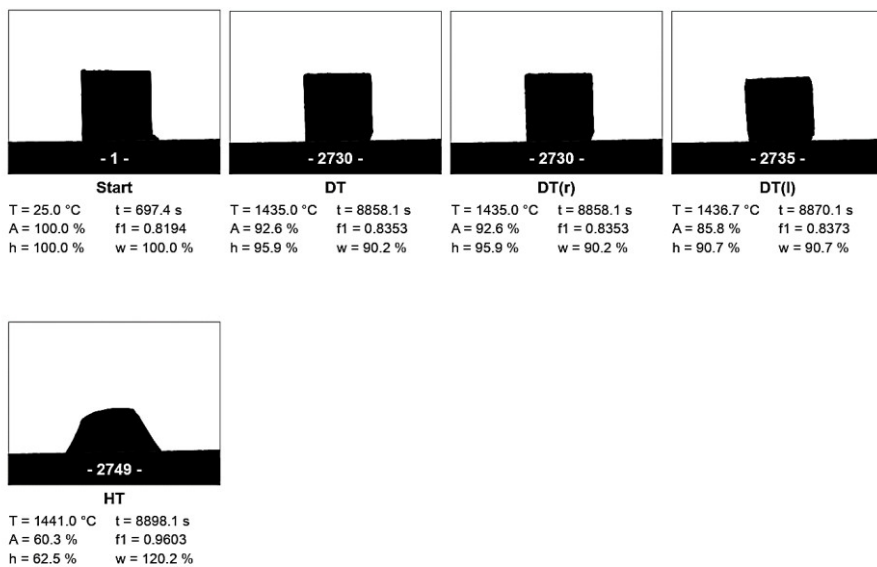
Figure Appendix 1. Silhouettes of slag sample 1 during heating-up in the hot stage microscope



Legend

T Temperature
t Time
A Area
f1 Aspect ratio 1
h Height
w Width

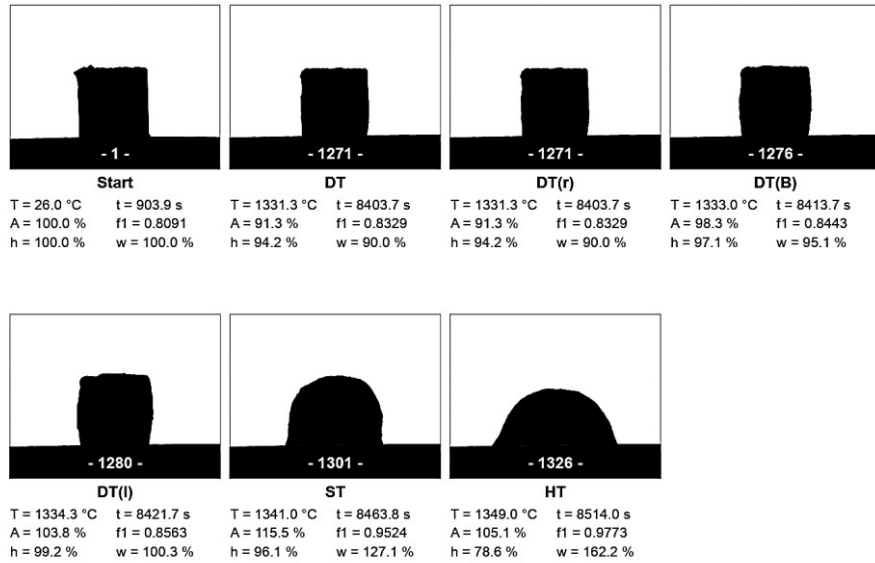
Figure Appendix 2. Silhouettes of slag sample 2 during heating-up in the hot stage microscope



Legend

T Temperature
t Time
A Area
f1 Aspect ratio 1
h Height
w Width

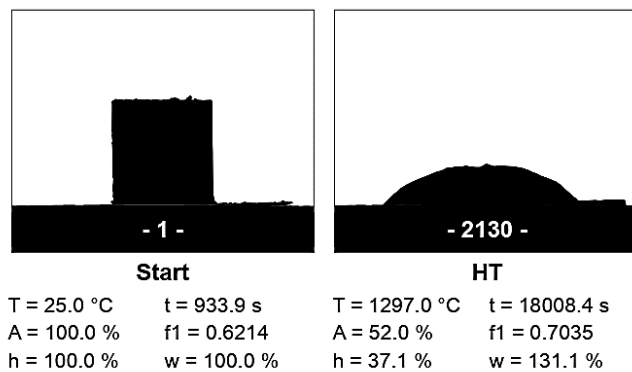
Figure Appendix 3. Silhouettes of slag sample 3 during heating-up in the hot stage microscope



Legend

T Temperature
t Time
A Area
f1 Aspect ratio 1
h Height
w Width

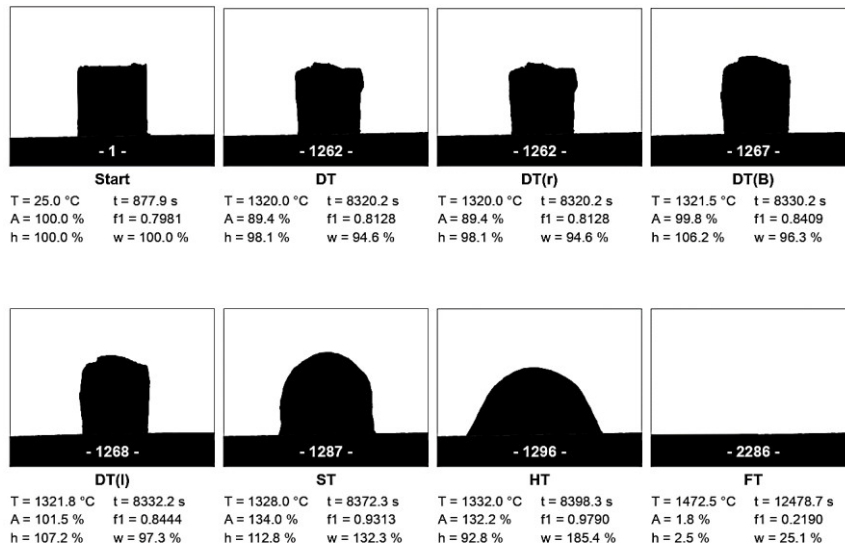
Figure Appendix 4. Silhouettes of slag sample 4 during heating-up in the hot stage microscope



Legend

T Temperature
t Time
A Area
f1 Aspect ratio 1
h Height
w Width

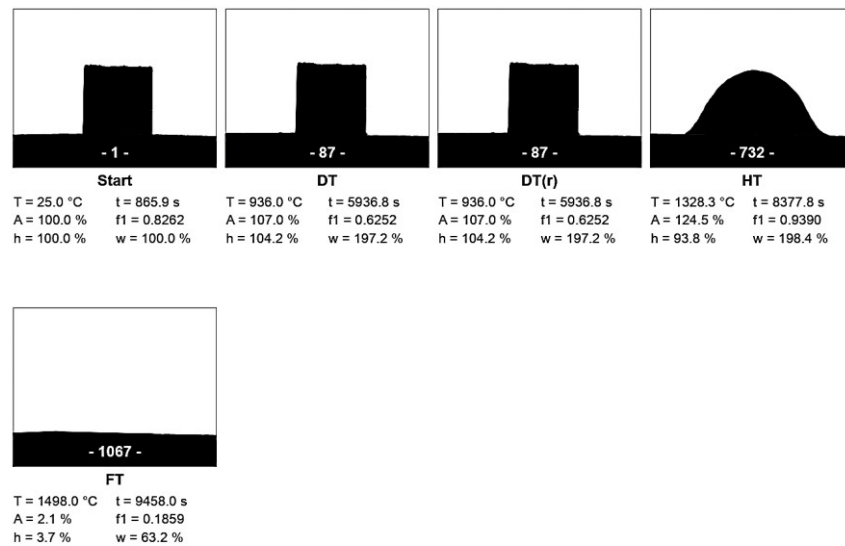
Figure Appendix 5. Silhouettes of slag sample 5 during heating-up in the hot stage microscope



Legend

T Temperature
t Time
A Area
f1 Aspect ratio 1
h Height
w Width

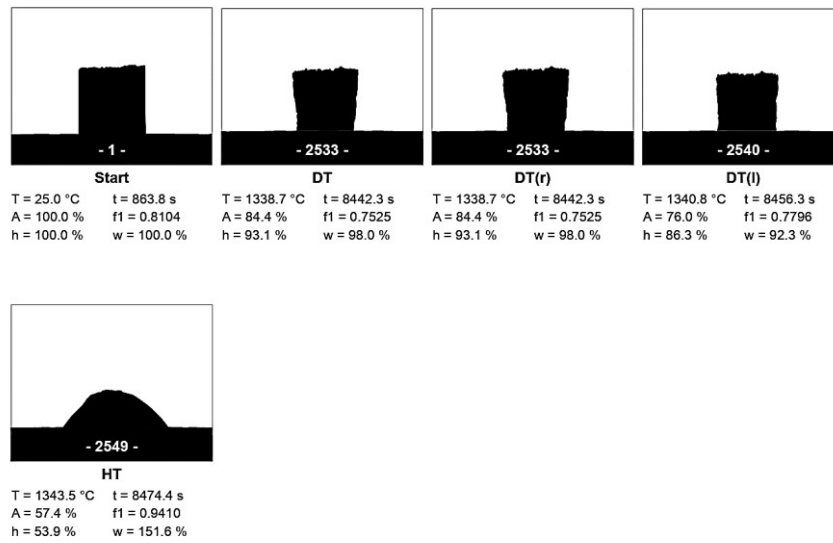
Figure Appendix 6. Silhouettes of slag sample 6 during heating-up in the hot stage microscope



Legend

T Temperature
t Time
A Area
f1 Aspect ratio 1
h Height
w Width

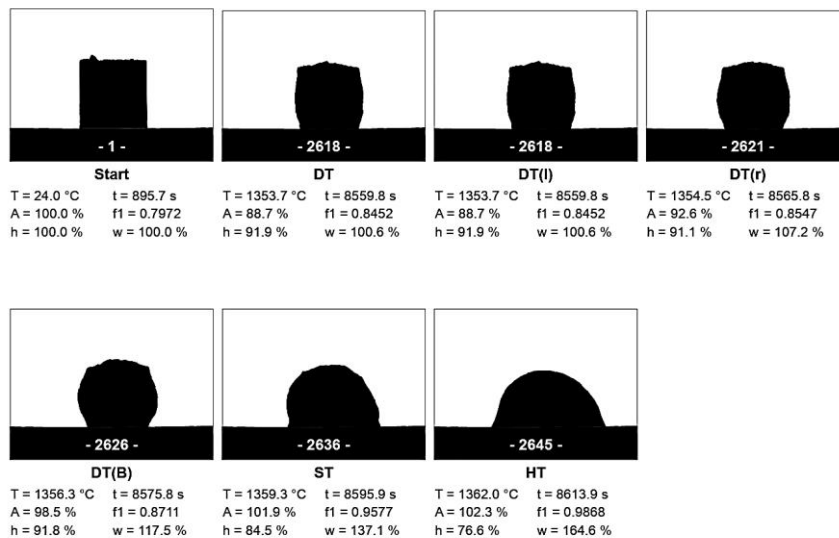
Figure Appendix 7. Silhouettes of slag sample 6 during heating-up in the hot stage microscope



Legend

T Temperature
t Time
A Area
f1 Aspect ratio 1
h Height
w Width

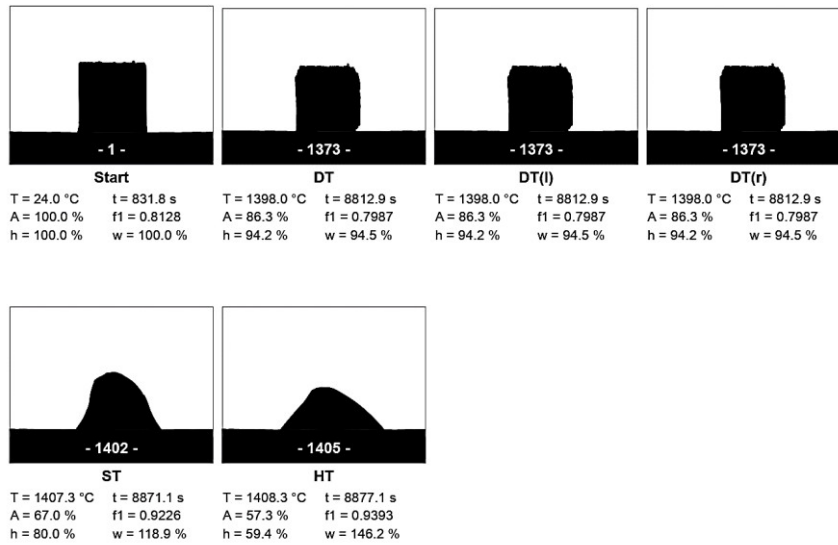
Figure Appendix 8. Silhouettes of slag sample 7 during heating-up in the hot stage microscope



Legend

T Temperature
t Time
A Area
f1 Aspect ratio 1
h Height
w Width

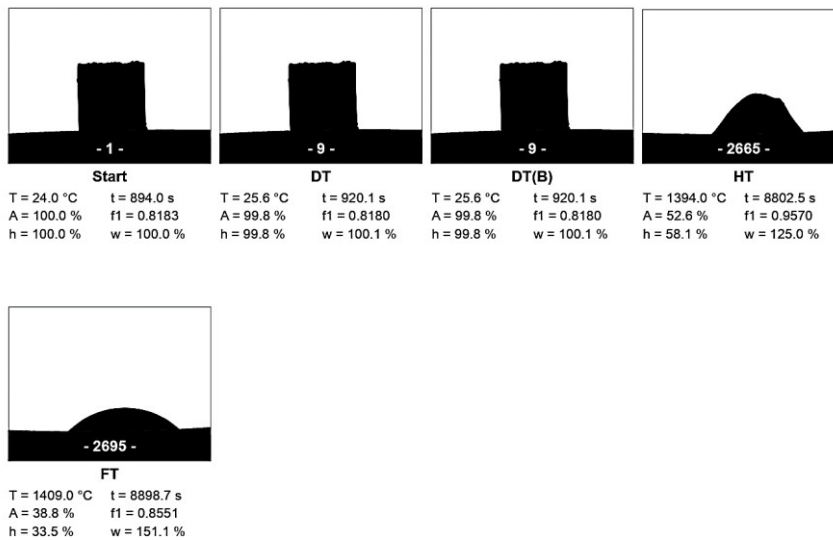
Figure Appendix 9. Silhouettes of slag sample 8 during heating-up in the hot stage microscope



Legend

T Temperature
t Time
A Area
f1 Aspect ratio 1
h Height
w Width

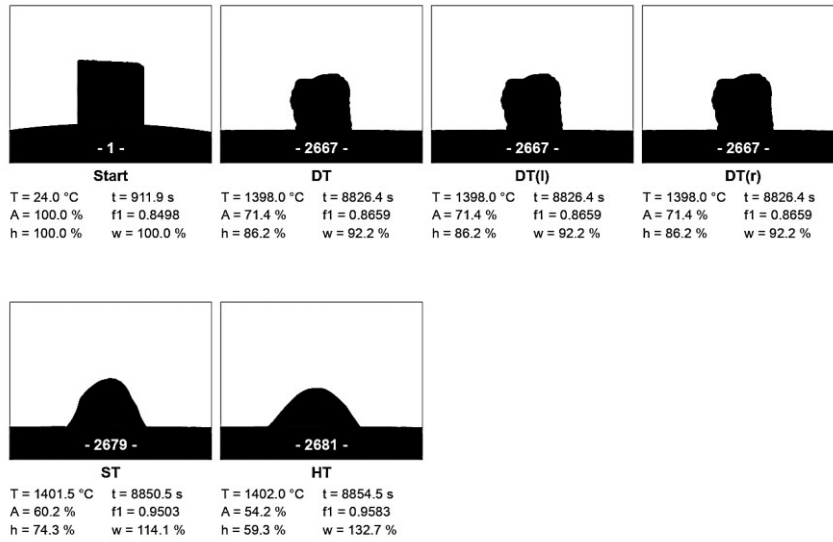
Figure Appendix 10. Silhouettes of slag sample 11 during heating-up in the hot stage microscope



Legend

T Temperature
t Time
A Area
f1 Aspect ratio 1
h Height
w Width

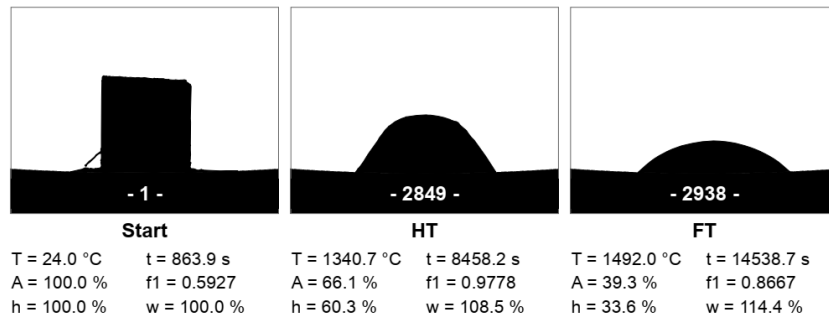
Figure Appendix 11. Silhouettes of slag sample 12 during heating-up in the hot stage microscope



Legend

T Temperature
t Time
A Area
f1 Aspect ratio 1
h Height
w Width

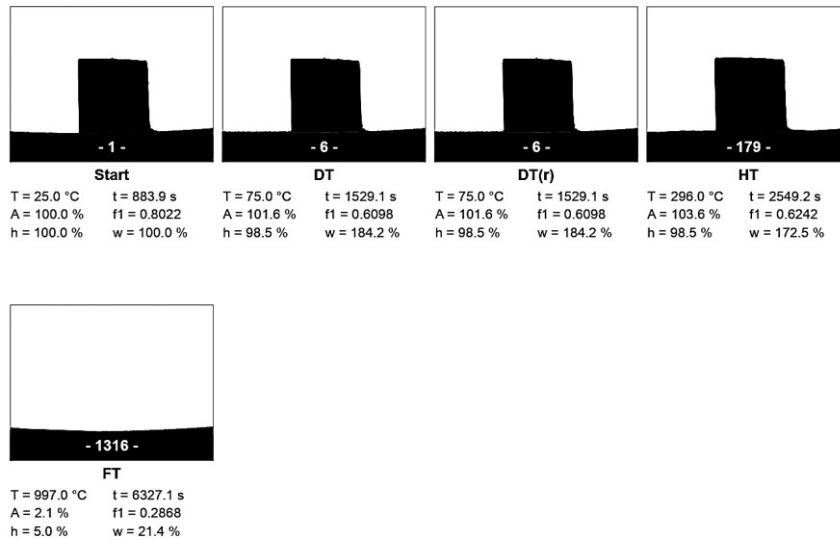
Figure Appendix 12. Silhouettes of slag sample 13 during heating-up in the hot stage microscope



Legend

T Temperature
t Time
A Area
f1 Aspect ratio 1
h Height
w Width

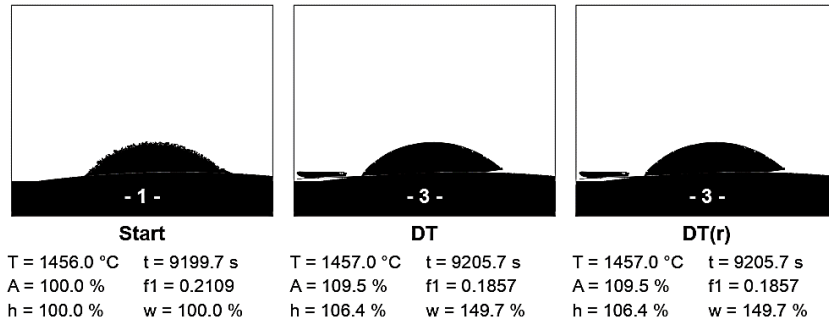
Figure Appendix 13. Silhouettes of slag sample 14 during heating-up in the hot stage microscope



Legend

T Temperature
t Time
A Area
f1 Aspect ratio 1
h Height
w Width

Figure Appendix 14. Silhouettes of slag sample 15 during heating-up in the hot stage microscope



Legend

T Temperature
t Time
A Area
f1 Aspect ratio 1
h Height
w Width

Figure Appendix 15. Silhouettes of slag sample 16 during heating-up in the hot stage microscope

10.2 Appendix B – Measured Data of the Slag Samples

Table Appendix 1. Measured data of slag sample 1

Measured Data, wt.-%				
Analyzed Point	Ce ₂ O ₃	SiO ₂	CaO	Total
Spektrum 8	58.82	23.54	17.64	100.00
Spektrum 9	6.89	43.73	49.38	100.00
Spektrum 10	6.73	44.49	48.78	100.00
Spektrum 13	11.31	32.81	55.88	100.00
Spektrum 14	48.27	28.33	23.40	100.00

Table Appendix 2. Measured data of slag sample 2

Measured Data, wt.-%					
Analyzed Point	Ce ₂ O ₃	SiO ₂	CaO	MgO	Total
Spektrum 4	35.23	42.96	21.81	0.00	100.00
Spektrum 5	0.00	53.01	44.18	2.82	100.00
Spektrum 8	35.52	43.69	20.78	0.00	100.00
Spektrum 9	0.00	55.40	25.88	18.73	100.00

Table Appendix 3. Measured data of slag sample 3

Measured Data, wt.-%					
Analyzed Point	Ce ₂ O ₃	SiO ₂	CaO	MgO	Total
Spektrum 1	0.00	36.29	51.24	12.47	100.00
Spektrum 2	0.00	43.78	41.55	14.68	100.00
Spektrum 3	62.85	22.87	14.28	0.00	100.00
Spektrum 4	63.07	22.58	14.36	0.00	100.00
Spektrum 5	14.87	49.52	15.03	20.57	100.00
Spektrum 6	0.00	36.60	51.14	12.25	100.00
Spektrum 7	17.04	49.21	12.24	21.52	100.00
Spektrum 8	61.77	23.61	14.62	0.00	100.00
Spektrum 9	23.31	46.32	11.68	18.68	100.00
Spektrum 10	61.17	23.97	14.86	0.00	100.00
Spektrum 11	0.00	43.83	41.47	14.70	100.00
Spektrum 12	0.00	43.59	41.57	14.84	100.00
Spektrum 13	0.00	36.55	51.21	12.24	100.00
Spektrum 14	0.00	36.40	51.26	12.34	100.00

Table Appendix 4. Measured data of slag sample 4

Measured Data, wt.-%					
Analyzed Point	Ce ₂ O ₃	SiO ₂	CaO	MgO	Total
Spektrum 1	0.00	100.00	0.00	0.00	100.00
Spektrum 2	5.58	57.02	27.14	10.26	100.00
Spektrum 3	5.74	57.03	26.93	10.31	100.00
Spektrum 4	0.00	100.00	0.00	0.00	100.00
Spektrum 5	0.00	100.00	0.00	0.00	100.00
Spektrum 6	5.58	57.34	27.00	10.07	100.00
Spektrum 7	5.60	57.01	27.09	10.30	100.00
Spektrum 8	0.00	100.00	0.00	0.00	100.00

Table Appendix 5. Measured data of slag sample 5

Measured Data, wt.-%					
Analyzed Point	Ce ₂ O ₃	SiO ₂	CaO	MgO	Total
Spektrum 1	5.95	56.36	35.54	2.15	100.00
Spektrum 2	0.00	100.00	0.00	0.00	100.00
Spektrum 3	5.38	57.06	35.13	2.43	100.00
Spektrum 4	0.00	97.41	2.59	0.00	100.00
Spektrum 5	0.00	100.00	0.00	0.00	100.00

Table Appendix 6. Measured data of slag sample 7

Measured Data, wt.-%					
Analyzed Point	Ce ₂ O ₃	SiO ₂	CaO	MgO	Total
Spektrum 1	8.40	54.53	29.83	7.23	100.00
Spektrum 2	0.34	44.09	41.22	14.35	100.00
Spektrum 3	8.46	54.20	29.63	7.71	100.00
Spektrum 4	0.00	44.38	41.27	14.35	100.00

Table Appendix 7. Measured data of slag sample 8

Measured Data, wt.-%					
Analyzed Point	Ce ₂ O ₃	SiO ₂	CaO	MgO	Total
Spektrum 1	0.00	43.44	2.07	54.49	100.00
Spektrum 2	0.00	43.10	1.83	55.07	100.00
Spektrum 3	6.58	48.91	32.66	11.85	100.00
Spektrum 4	6.08	48.74	31.47	13.71	100.00
Spektrum 5	6.26	48.81	30.99	13.93	100.00
Spektrum 6	0.00	43.04	1.82	55.14	100.00

Table Appendix 8. Measured data of slag sample 9

Measured Data, wt.-%						
Analyzed Point	Ce ₂ O ₃	SiO ₂	CaO	MgO	Al ₂ O ₃	Total
Spektrum 1	98.89	0.00	1.11	0.00	0.00	100.00
Spektrum 2	97.64	0.00	2.17	0.00	0.19	100.00
Spektrum 3	5.51	42.30	34.38	6.21	11.61	100.00
Spektrum 4	5.88	41.91	35.11	5.44	11.67	100.00
Spektrum 5	0.22	38.64	35.30	25.83	0.00	100.00
Spektrum 6	0.57	37.95	35.46	26.02	0.00	100.00
Spektrum 7	1.35	36.57	49.98	12.10	0.00	100.00
Spektrum 8	1.68	35.59	50.84	11.89	0.00	100.00

Table Appendix 9. Measured data of slag sample 10

Measured Data, wt.-%						
Analyzed Point	Ce ₂ O ₃	SiO ₂	CaO	MgO	Al ₂ O ₃	Total
Spektrum 1	17.61	37.10	19.64	8.98	16.67	100.00
Spektrum 2	20.86	36.15	16.47	10.18	16.35	100.00
Spektrum 3	0.00	42.46	3.37	54.17	0.00	100.00
Spektrum 4	0.00	42.09	4.18	53.73	0.00	100.00
Spektrum 5	0.00	42.22	41.01	13.42	3.36	100.00
Spektrum 6	0.00	41.57	41.41	13.06	3.95	100.00
Spektrum 7	0.00	36.45	51.13	12.41	0.00	100.00
Spektrum 8	0.00	41.65	40.99	12.72	4.64	100.00
Spektrum 9	0.00	41.54	41.03	13.17	4.26	100.00
Spektrum 10	0.00	42.48	2.70	54.82	0.00	100.00
Spektrum 11	15.82	37.39	19.59	9.39	17.82	100.00
Spektrum 12	16.78	37.63	17.83	11.14	16.62	100.00

Table Appendix 10. Measured data of slag sample 11

Measured Data, wt.-%						
Analyzed Point	Ce ₂ O ₃	SiO ₂	CaO	MgO	Al ₂ O ₃	Total
Spektrum 1	1.84	43.17	38.15	7.35	9.49	100.00
Spektrum 2	0.00	36.19	51.35	12.47	0.00	100.00
Spektrum 3	0.00	36.38	51.14	12.48	0.00	100.00
Spektrum 4	1.96	43.41	38.59	6.37	9.68	100.00
Spektrum 5	0.00	38.26	35.34	26.40	0.00	100.00
Spektrum 6	0.00	38.09	35.94	25.97	0.00	100.00
Spektrum 7	0.00	38.38	34.15	27.47	0.00	100.00
Spektrum 8	1.72	43.39	36.33	10.24	8.33	100.00
Spektrum 9	1.61	43.17	36.46	10.07	8.70	100.00
Spektrum 10	0.00	36.40	51.20	12.40	0.00	100.00
Spektrum 11	0.00	36.27	51.31	12.42	0.00	100.00
Spektrum 12	0.00	38.33	34.39	27.28	0.00	100.00
Spektrum 13	0.00	38.27	35.68	26.06	0.00	100.00

Table Appendix 11. Measured data of slag sample 12

Measured Data, wt.-%						
Analyzed Point	Ce ₂ O ₃	SiO ₂	CaO	MgO	Al ₂ O ₃	Total
Spektrum 1	0.00	38.01	35.98	26.01	0.00	100.00
Spektrum 2	100.00	0.00	0.00	0.00	0.00	100.00
Spektrum 3	100.00	0.00	0.00	0.00	0.00	100.00
Spektrum 4	100.00	0.00	0.00	0.00	0.00	100.00
Spektrum 6	0.00	38.56	35.67	25.76	0.00	100.00
Spektrum 9	0.00	38.30	35.92	25.77	0.00	100.00
Spektrum 10	0.00	38.10	36.14	25.76	0.00	100.00
Spektrum 11	5.79	50.41	24.29	6.48	13.03	100.00
Spektrum 12	0.00	36.65	51.29	12.06	0.00	100.00
Spektrum 13	0.00	35.90	52.24	11.86	0.00	100.00
Spektrum 14	0.00	36.44	51.19	12.37	0.00	100.00
Spektrum 15	4.87	43.61	34.20	5.91	11.41	100.00
Spektrum 33	0.00	36.39	51.66	11.95	0.00	100.00
Spektrum 34	0.00	38.29	36.60	25.11	0.00	100.00
Spektrum 35	0.00	38.26	35.53	26.21	0.00	100.00
Spektrum 36	0.00	38.18	36.15	25.67	0.00	100.00
Spektrum 38	100.00	0.00	0.00	0.00	0.00	100.00
Spektrum 39	100.00	0.00	0.00	0.00	0.00	100.00
Spektrum 43	0.00	36.46	51.31	12.23	0.00	100.00
Spektrum 46	4.99	43.86	33.68	6.24	11.23	100.00
Spektrum 48	4.63	43.34	36.23	4.59	11.20	100.00

Table Appendix 12. Measured data of slag sample 13

Measured Data, wt.-%						
Analyzed Point	Ce ₂ O ₃	SiO ₂	CaO	MgO	Al ₂ O ₃	Total
Spektrum 49	3.95	44.14	36.36	5.43	10.12	100.00
Spektrum 52	0.00	38.69	35.60	25.71	0.00	100.00
Spektrum 53	0.00	35.85	41.91	22.23	0.00	100.00
Spektrum 54	0.00	38.71	35.11	26.19	0.00	100.00
Spektrum 56	0.00	38.59	34.76	26.65	0.00	100.00
Spektrum 57	3.76	43.56	35.65	5.66	11.37	100.00
Spektrum 59	0.00	36.38	51.70	11.92	0.00	100.00
Spektrum 60	0.00	36.83	50.99	12.19	0.00	100.00
Spektrum 61	0.00	38.51	33.95	27.54	0.00	100.00
Spektrum 62	0.00	38.39	35.79	25.81	0.00	100.00
Spektrum 63	0.00	36.42	51.53	12.05	0.00	100.00
Spektrum 64	3.88	42.47	37.74	5.49	10.42	100.00
Spektrum 65	0.00	37.76	38.18	24.05	0.00	100.00
Spektrum 66	0.00	38.68	34.47	26.85	0.00	100.00

Measured Data, wt.-%						
Analyzed Point	Ce ₂ O ₃	SiO ₂	CaO	MgO	Al ₂ O ₃	Total
Spektrum 68	63.76	18.52	10.90	6.82	0.00	100.00
Spektrum 75	4.20	43.91	35.47	5.39	11.02	100.00
Spektrum 76	3.64	43.75	35.76	5.49	11.36	100.00
Spektrum 77	0.00	36.78	51.21	12.01	0.00	100.00
Spektrum 78	0.00	36.61	51.29	12.09	0.00	100.00
Spektrum 79	0.00	42.37	36.66	13.17	7.80	100.00

Table Appendix 13. Measured data of slag sample 14

Measured Data, wt.-%					
Analyzed Point	Ce ₂ O ₃	SiO ₂	CaO	MgO	Total
Spektrum 107	2.46	59.31	28.43	9.79	100.00
Spektrum 108	2.13	59.88	28.28	9.72	100.00
Spektrum 109	2.04	57.13	31.40	9.43	100.00
Spektrum 110	2.09	59.03	30.00	8.89	100.00
Spektrum 111	1.87	59.72	29.15	9.26	100.00

Table Appendix 14. Measured data of slag sample 15

Measured Data, wt.-%					
Analyzed Point	Ce ₂ O ₃	SiO ₂	CaO	MgO	Total
Spektrum 164	0.00	60.57	30.89	8.54	100.00
Spektrum 165	1.04	60.11	30.32	8.53	100.00
Spektrum 166	1.15	59.79	30.57	8.49	100.00
Spektrum 167	0.00	60.47	30.75	8.78	100.00
Spektrum 168	0.00	60.95	30.71	8.35	100.00
Spektrum 169	1.05	60.28	30.12	8.55	100.00
Spektrum 170	1.04	60.14	30.67	8.15	100.00

Table Appendix 15. Measured data of slag sample 16

Measured Data, wt.-%					
Analyzed Point	Ce ₂ O ₃	SiO ₂	CaO	MgO	Total
Spektrum 229	0.00	35.67	52.53	11.80	100.00
Spektrum 230	0.00	38.07	37.35	24.59	100.00
Spektrum 231	0.00	35.54	52.79	11.67	100.00
Spektrum 232	2.16	48.62	42.13	7.09	100.00
Spektrum 233	1.95	47.13	44.20	6.72	100.00
Spektrum 236	0.00	38.44	35.66	25.91	100.00
Spektrum 237	0.00	38.37	37.58	24.05	100.00
Spektrum 238	0.00	37.90	36.91	25.18	100.00
Spektrum 239	0.00	38.32	36.67	25.01	100.00

Measured Data, wt.-%					
Analyzed Point	Ce ₂ O ₃	SiO ₂	CaO	MgO	Total
Spektrum 241	1.70	48.29	44.06	5.94	100.00
Spektrum 242	1.59	48.04	43.12	7.25	100.00
Spektrum 243	0.00	35.48	52.90	11.62	100.00
Spektrum 246	1.72	48.28	44.01	5.99	100.00
Spektrum 247	1.17	43.02	48.06	7.76	100.00

Note:

(*) Proposed formula

(**) inclusive dissolved Ce₂O₃